Fractal, Logarithmic, and Volume-Law Entangled Nonthermal Steady States via Spacetime Duality

Matteo Ippoliti⬤, Tibor Rakovszky, and Vedika Khemani

Department of Physics, Stanford University, Stanford, California 94305, USA

The extension of many-body quantum dynamics to the nonunitary domain has led to a series of exciting developments, including new out-of-equilibrium entanglement phases and phase transitions. We show how a duality transformation between space and time, on one hand, and unitarity and nonunitarity, on the other, can be used to realize steady-state phases of nonunitary dynamics that exhibit a rich variety of behavior in their entanglement scaling with subsystem size—from logarithmic to extensive to *fractal*. We show how these outcomes in nonunitary circuits (that are "spacetime dual" to unitary circuits) relate to the growth of entanglement in time in the corresponding unitary circuits, and how they differ, through an exact mapping to a problem of unitary evolution with boundary decoherence, in which information gets "radiated away" from one edge of the system. In spacetime duals of chaotic unitary circuits, this mapping allows us to analytically derive a nonthermal volume-law entangled phase with a universal logarithmic correction to the entropy, previously observed in unitary-measurement dynamics. Notably, we also find robust steady-state phases with fractal entanglement scaling, $S(\ell) \sim \ell^\alpha$ with tunable $0 < \alpha < 1$ for subsystems of size ℓ in one dimension. We present an experimental protocol for preparing these novel steady states with only a vanishing density of postselected measurements via a type of "teleportation" between spacelike and timelike slices of quantum circuits.

I. INTRODUCTION

Breakthrough experimental advances in building quantum simulators have opened up new regimes in the study of many-body physics, by providing direct access to the dynamics of quantum systems. This has advanced our understanding of many foundational questions ranging from the onset of chaos and thermalization, to many-body localization, to the definition of phase structure out of equilibrium [1–4]. A unifying theme in these explorations has been the study of many-body quantum entanglement across a wide variety of settings—eigenstates of stationary Hamiltonians or of periodically driven (Floquet) evolutions; out-of-equilibrium states in driven or postquench dynamics; and, more recently, steady-state ensembles of *nonunitary* "monitored" circuits which combine unitary evolution with local nonunitary measurements (the unitary part can also be dispensed with in "measurement-only" circuits) [5–14]. The exploration of nonunitary dynamics is particularly topical in the age of noisy, intermediate-scale

quantum simulators [15], which naturally include nonunitary ingredients in two ways: on the one hand, by the presence of (uncontrolled) environmental noise and decoherence; on the other, by allowing controlled quantum measurements *during* the dynamics (a key capability for error correction in future "fault-tolerant" quantum computers).

In both unitary and nonunitary cases, both the *growth of entanglement in time*, as well as its *spatial scaling*, may show interesting structure, including sharp phase transitions between distinct behaviors. A paradigmatic example is the many-body-localized (MBL) phase [2,16,17], where entanglement growth is only logarithmic in time [18–20]; this sharply transitions to a faster algebraic (though potentially sub-ballistic [21–25]) growth at an MBL-to-thermalizing transition. Monitored nonunitary circuits, on the other hand, feature sharp transitions in the spatial scaling of their steady-state entanglement [5–9]: from an area law (at high measurement rate) to a volume law (at low enough rate), through a logarithmically entangled critical point described by a conformal field theory (CFT) [26–29]. In all, we are only beginning to explore the rich variety of novel phenomena displayed by the *dynamics* of many-body systems, and our understanding of most questions in this domain, particularly in the nonunitary setting, is still nascent.

In this work, we add to this understanding by studying entanglement dynamics in a new class of nonunitary evolutions—those that are "spacetime duals" of unitary circuits—recently introduced by two of us [30]. Spacetime duality, in simple terms, exchanges the roles of space and time in a quantum evolution and (generically) associates to every unitary circuit a nonunitary partner. Dualities reveal connections between seemingly distinct problems, and they often point to entirely *new* results or phenomena—Wegner's gauge-spin duality being a paradigmatic example [31]; this case is no exception.

Our work makes three main advances.

(i) First, we present new classes of steady-state phases for entanglement dynamics. These include, most notably, a robust family of *fractally entangled* steady-state phases that lie outside the established classifications of "area-law," "volume-law," or logarithmic entanglement scaling generically exhibited by the eigenstates or steady states of unitary quantum dynamics [32].

(ii) Second, our results are obtained via a method that is interesting in and of itself. The spacetime-duality transformation allows us to build on the existing body of knowledge on entanglement dynamics in unitary circuits and, thus, affords a powerful analytical handle on the study of nonunitary dynamics that is otherwise missing away from special limits. [40] In particular, we analytically derive a universal subleading logarithmic correction to the entanglement of nonthermal volume-law steady states that exactly realizes the conjectured universal behavior of unitary-projective circuits in the entangling phase [42,43]; this log-correction is key to our understanding of the volume-law phase as a type of dynamically generated error-correcting code, which hides information form local measurements and, thus, allows entanglement to survive [8,9].

(iii) Third, on the experimental side, our work opens up new ways for more efficient realizations of measurement-induced phases in experiments. In particular, we show how the steady states of spacetime-dual circuits can be obtained with an exponentially smaller "postselection overhead" (explained below), which is a central practical challenge associated with preparing many-body states that realize measurement-induced phases.

We now give a slightly more detailed outline of these ideas. One of the main objects of this work is to explore the relationship between entanglement in spacetime-dual partner circuits—or, more precisely, between *entanglement dynamics* in the unitary circuit and *spatial scaling of entanglement* in late-time states of its nonunitary dual. Unitary dynamics gives rise to a variety of possible behaviors for entanglement growth. The nonunitary dual circuits inherit this variety and, thus, display a similar
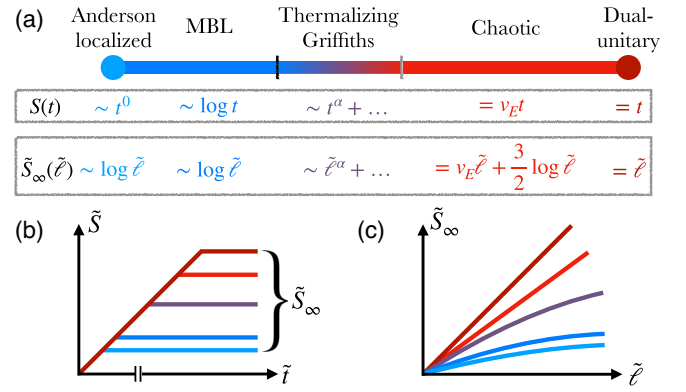

FIG. 1. Summary of various dynamical regimes in unitary circuits and properties of steady states in their spacetime duals. (a) Regimes from least to most entangling. First row: growth of entanglement in time, $S(t)$, in unitary circuits of each type. Second row: scaling of entanglement with subsystem size $\tilde{\ell}$ in the steady state of the spacetime-dual circuit, $\tilde{S}_\infty$. The two agree up to logarithmic terms, which dominate for Anderson-localized circuits. In the Griffiths regime, only the leading-order term is shown; for other cases, the results are expected to be exact up to terms at most constant in $\tilde{\ell}$. (b) Growth of $\tilde{S}$ in the spacetime-dual circuit: All regimes have ballistic growth with maximal speed at first ($\tilde{S} = \tilde{t}$) but saturate to different values. (c) Saturation value $\tilde{S}_\infty$ as a function of subsystem size $\tilde{\ell}$, going from logarithmic to ballistic, with arbitrary power law ($\tilde{S}_\infty \sim \tilde{\ell}^\alpha$, $0 < \alpha < 1$) in between.

wealth of steady-state phases characterized by different spatial entanglement scalings. Notably, some of the phases thus obtained go beyond the possibilities of generic unitary dynamics. Correspondingly, phase transitions in the growth of entanglement in unitary circuits (e.g., across an MBL transition) map onto phase transitions in the steady states of the spacetime-dual models.

A schematic summary of our work is shown in Fig. 1. We sweep through several classes of unitary evolutions, displaying the full range of behaviors for entanglement growth: from Anderson-localized circuits (where entanglement saturates to a constant [19]), to Floquet MBL [44–46] circuits (where it grows logarithmically [18–20,47]), then past an MBL-to-thermal phase transition to a slowly thermalizing phase (where entanglement is thought to grow sub-ballistically, as $\sim t^\alpha$ with $0 < \alpha < 1$, due to rare disorder-induced bottlenecks, so-called "Griffiths" effects [21–25]), all the way to generic chaotic circuits (where entanglement grows ballistically [48–50]). To leading approximation, each type of entanglement growth is mirrored in a distinct phase of a nonunitary circuit, characterized by the spatial scaling of entanglement at late times which ranges from logarithmic to fractal to volume law.

Most strikingly, the sub-ballistic entanglement growth in disordered, thermalizing systems translates to a fractal scaling of entanglement in steady states of a robust, generic class of nonunitary circuits. In these states, entropy scales

as a fractional, tunable power law of subsystem size (in one dimension) and is statistically self-similar over all length scales. These fractally entangled steady states are generically not obtained as either eigenstates or dynamical steady states in any unitary setting and represent a striking example of new, robust nonequilibrium phenomena made possible by adding nonunitarity to the toolkit of many-body quantum dynamics.

Separately, spacetime duality, as a theoretical tool, affords us a great degree of analytic tractability, which is key in understanding all these types of steady-state entanglement scaling. Specifically, we show that, for a unitary circuit U, the entanglement properties of states evolved by its (nonunitary) spacetime-dual circuit $\tilde{U}$ can be related to entanglement induced by U, with the roles of space and time exchanged, but with an additional twist: The unitary evolution is accompanied by *edge decoherence*, which allows information to escape the system and be "radiated away" from one of its edges. This is summarized by Eq. (1) below.

To leading order, as mentioned earlier, the growth of entanglement in time under U is mapped to the spatial scaling of steady-state entanglement under $\tilde{U}$, leading to the range of different scalings summarized in Fig. 1. Importantly, however, the interchanging of space and time is not the full story. The added twist of edge decoherence leaves its footprint in logarithmic contributions to the steady-state entanglement in the spacetime-dual circuit. This allows us to furnish an analytic derivation of universal subleading logarithmic corrections to nonthermal volume-law steady states. Identical corrections have been observed in unitary-measurement circuits [6] and found to be universal features of their nonthermal volume-law phase related to its quantum error-correcting properties [42,43]. Furthermore, the logarithmic correction may become the *leading* contribution in cases where one may naïvely expect area-law steady states (e.g., in duals of Anderson-localized models). Area-law steady states are, in fact, ruled out in spacetime duals of unitary circuits, barring trivial exceptions. Relatedly, the mapping to edge decoherence also allows us to prove that at short (dual) "times" the dual circuit $\tilde{U}$ produces *ballistic* growth of entanglement, at the maximum possible speed, even when the associated unitary circuit U is in a localized phase.

Finally, we note that spacetime duality is not only an interesting theoretical construct; it is also experimentally motivated. A crucial experimental challenge with realizing measurement induced phases is the "postselection overhead" associated with the measurements: Any nontrivial entanglement phase structure is displayed only by *individual* quantum trajectories [51] corresponding to pure states labeled by a fixed sequences of measurement outcomes, while it is lost in a stochastic mixture over measurement outcomes [5]. Experimentally measuring any observable feature of the output state requires reproducing the same

state multiple times (a single experimental run corresponds to a single "shot"); this requires us to fix (i.e., postselect) the sequence of measurement outcomes in order to reproduce a given output state, which creates a huge overhead for any finite density of measurements (exponential in the spacetime volume of the circuit) [52]. As shown in Ref. [30], the postselection cost can be significantly ameliorated (or, sometimes, eliminated altogether) when computing the purity of a (mixed) density matrix evolving under the spacetime duals of unitary circuits. A generalization of this idea also applies to the present context, where the (pure) steady states of interest can be prepared by using only local unitary gates and a limited number of postselected measurements scaling as the *boundary* of the circuit in spacetime—an exponential improvement over more conventional unitary-measurement setups [5,7]. We achieve this by "teleporting" the input and output states of dual circuits, which live on (experimentally unnatural) timelike surfaces, to spacelike surfaces that can be more readily accessed in experiments. We also discuss a family of experimentally realizable disordered Floquet Ising models with an MBL phase transition, whose spacetime duals display the full gamut of steady-state entanglement phases discussed above.

The balance of the paper is organized as follows. In Sec. II, we review the notion of spacetime duality and discuss how to realize spacetime duals of unitary circuits experimentally using only a vanishing density of projective measurements in spacetime. We then introduce the mapping to edge decoherence that serves as the main theoretical tool for the rest of the work. In Sec. III, we use this mapping to discuss duals of (Anderson- and many-body-) localized circuits and argue that steady-state entanglement diverges logarithmically with subsystem size in both cases. In Sec. IV, we turn to generic chaotic evolution, modeled by Haar-random circuits; we obtain volume-law entangled steady states, but with a universal nonthermal logarithmic correction stemming from the edge decoherence. Finally, in Sec. V, we consider slowly thermalizing models with sub-ballistic entanglement growth, mapped by spacetime duality to fractally entangled steady states. We summarize our results and discuss their implications for future research in Sec. VI.

II. SETUP

A. Nonunitary dynamics from spacetime duality

To review the idea of spacetime duality [30], we start from the simplest instance—that of a two-qudit unitary gate. Figures 2(a) and 2(b) illustrate how this one object, $U_{i_1 i_2}^{o_1 o_2}$ (unitarily mapping two inputs $i_{1,2}$ to two outputs $o_{1,2}$ according to "arrow of time" t), could alternatively be viewed "sideways," according to a rotated arrow of time $\tilde{t}$, as mapping input qubits i_1 and o_1 to output qubits i_2 and o_2. The resulting map, $\tilde{U}_{i_1 o_1}^{i_2 o_2}$—which we call the
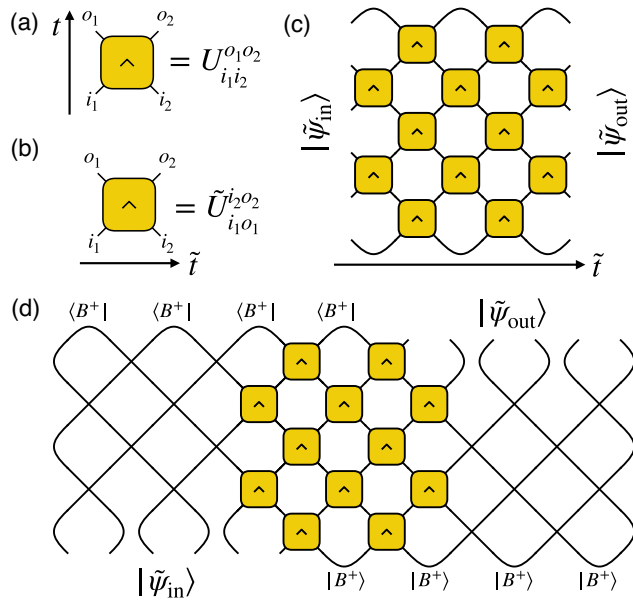
FIG. 2. Spacetime duality. (a) A two-qudit unitary gate U. Bottom legs are inputs; top legs are outputs. The caret symbol on the gate denotes the direction of unitarity. (b) If we follow the arrow of time $\tilde{t}$ (left to right), the same object describes a nonunitary operation $\tilde{U}$. (c) Spacetime dual of a brickwork unitary circuit: The nonunitary gates $\tilde{U}$ turn the input state $|\tilde{\psi}_{\text{in}}\rangle$ (at the left boundary) into the output state $|\tilde{\psi}_{\text{out}}\rangle$ (at the right boundary). Both states exist on timelike surfaces. (d) The input and output states can be "teleported" to spacelike surfaces by employing ancillas initialized in a Bell-pair state $|B^{+}\rangle = q^{-1/2}\sum_{i=1}^{q}|ii\rangle$, SWAP gates, and postselected projective measurements on $\langle B^{+}|$. The number of postselected measurements is proportional to the length of the circuit's boundary.

"(spacetime)-dual" or "(spacetime)-flipped" version of U—is, in general, *not* unitary.

For example, if U is a two-site identity gate, its dual $\tilde{\mathbb{1}} = q|B^{+}\rangle\langle B^{+}|$ is proportional to a projection onto the Bell-pair state $|B^{+}\rangle \equiv q^{-1/2}\sum_{a=1}^{q}|aa\rangle$ (q is the local Hilbert space dimension). Notice that this is a *forced* measurement: The measurement outcome is fixed. In general, a polar decomposition yields $\tilde{U} = qFW$, where W is a unitary gate and F is positive semidefinite and normalized to $\text{Tr}(F^2) = 1$. Since $F \geq 0$, we can interpret $\tilde{U}$ as an element of a positive operator-valued measure (POVM): It corresponds to a *forced weak measurement* (i.e., deterministically postselecting a particular outcome of a POVM); alternatively, one could think of F as finite-time imaginary time evolution with a two-site Hamiltonian.

We note that the use of forced measurements (rather than Born-random quantum measurements) does not obstruct the existence of measurement-induced entanglement phases and transitions. Deep in an entangling phase, with very infrequent measurements, outcomes are expected to be uniformly distributed, so that forced measurements should be equivalent to typical trajectories of random

measurements [42]. In Clifford circuits, measurement outcomes yield "phase bits" that do not affect entanglement [55,56] (provided the outcomes are mutually compatible [57]). More generally, forced and random measurements are thought to give rise to the same qualitative phenomenology (with specific quantitative differences in criticality [41] and late-time dynamics [58]).

Having defined how spacetime duality acts on individual gates, it is straightforward to extend the idea to $1 + 1$-dimensional circuits made out of two-site unitary gates in a "brick-wall" pattern [30]. This idea of flipping circuits is at the core of much recent work on a variety of topics. In particular, important analytical progress on quantum chaos has been achieved via special *dual-unitary* circuits [59–68], where each gate U making up the circuit is such that $\tilde{U}$ happens to be unitary as well. More generically, other works explore the idea of using the spacetime-flipped circuits as a tool for calculating properties of the original unitary evolution, with applications ranging from tensor network contractions [69–72] to MBL [73–75] to chaos and thermalization [76–78]. On the other hand, Ref. [30] (by a subset of us) introduces the idea of using spacetime duality to a different end—not to understand features of the associated unitary evolution but rather to study the nonunitary dynamics in its own right. Here, we build on this to engineer new phases and phenomena, such as exotic nonthermal steady states.

For consistency, when drawing circuit diagrams we always choose the direction of (unitary) time t as bottom to top (also indicated by a small arrowhead symbol on each gate), while the "dual" arrow of time $\tilde{t}$ flows left to right. [79] The spacetime dual of a unitary circuit thus evolves states sideways, left to right.

This may seem to pose a conceptual issue, since the input and output states $|\tilde{\psi}_{\text{in/out}}\rangle$ (both pure) exist on *timelike* (vertical) slices of the circuit [Fig. 2(c)]. However, this can be remedied, as shown in Fig. 2(d). The idea is to "teleport" the input and output states from their native timelike surface to spacelike ones [80] by using ancillary qudits arranged in 1D (the half of these on the right are initialized in Bell-pair states $|B^{+}\rangle$), a brick-wall pattern of SWAP gates that extends the original unitary circuit on the left and right, [81] and measurements only at the end of the unitary time evolution. The upshot is that an experimentalist can obtain the desired target output state of the dual nonunitary evolution by simply performing a (suitably modified) unitary evolution, followed by a set of measurements only at the final time. These final measurements implement the "upside-down" Bell pairs at the top of the circuit in Fig. 2(d), which represent open boundary conditions for the flipped circuit [82].

As mentioned above, these Bell measurements are forced, or postselected—the experimentalist performs a Bell measurement and discards any realizations where the outcome is not $|B^{+}\rangle$. However, we note two advantageous

features of this setup, compared to more generic unitary-measurement circuits. First, the measurements all take place at the end of the circuit rather than in the middle; this is useful, as some quantum simulator architectures do not allow measurements in the middle of a circuit (measurements can be deferred to the end of the circuit, at the expense of injecting a growing number of ancillas [54]). Second, the number of forced or postselected measurements scales only with the circuit's *boundary* rather than its spacetime volume. Thus, spacetime duality presents a way to realize interesting nonunitary circuits with a drastically reduced postselection overhead.

This overhead is further ameliorated by a suitable choice of initial states: If $|\tilde{\psi}_{in}\rangle$ is set to be a product of nearest-neighbor Bell pairs, then we can get rid of the ancillas on the left in Fig. 2(d), since this particular choice of initial condition is automatically realized by simply taking open boundary conditions on the left edge of the associated unitary circuit, as depicted in Fig. 3(a). In the following, we focus on such Bell-pair initial states. In addition to lowering the postselection overhead, this ensures that, in the thermodynamic limit $\tilde{L} \to \infty$, the state $|\tilde{\psi}_{out}\rangle$ maintains its normalization at all times, despite the flipped circuit being nonunitary, as we prove in Appendix A.

B. Mapping to boundary decoherence

We now discuss the connection between entanglement dynamics in the unitary circuit and spatial scaling of entanglement in its spacetime dual. This connection is made crisp by an exact mapping to a problem of unitary evolution with "edge decoherence" that we present below, with some further technical details in Appendix A.

Before we begin, let us fix some conventions and notation. We denote by L and T the size (number of qudits) and depth (number of gate layers) of the unitary circuit, respectively, and by $\tilde{L}$ and $\tilde{T}$ the size and depth, respectively, of its (nonunitary) spacetime dual; these obey $L = \tilde{T}$ and $T = \tilde{L}$. We denote by $\tilde{S}$ the entanglement entropy of a timelike (vertical) subsystem [for instance, region A in Fig. 3(a)] and by S the entropy of a spacelike (horizontal) subsystem [for instance, region B in Fig. 3(a)]. The on-site Hilbert space dimension is q (in most cases below, $q = 2$).

Our main goal is to understand the entanglement properties of the late-time output states of the flipped circuit. We focus on the entropy of contiguous subsystems near one edge, denoted by A, with size $|A| \equiv \tilde{\ell}$. The complementary subsystem $\bar{A}$ consists of $\tilde{L} - \tilde{\ell}$ sites. This setup is illustrated in Fig. 3(a). We denote the (von Neumann or Rényi) entropy of region A by $\tilde{S}(\tilde{T}, \tilde{\ell})$.

The setup is considerably simplified if we take the thermodynamic limit $\tilde{L} \to \infty$. As we show next, in this limit the entropy of A can be given a very useful alternative characterization in terms of the original unitary dynamics
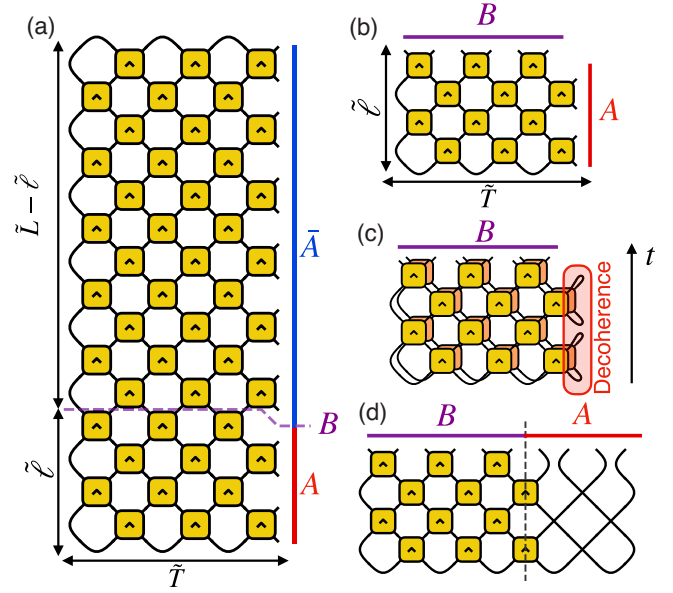

FIG. 3. Mapping the entropy of the spacetime-dual circuit's output state to that of unitary dynamics with boundary decoherence. (a) Setup: We fix the input state $|\tilde{\psi}_{in}\rangle$ to be a product of Bell pairs (open boundary, left), and the output state $|\tilde{\psi}_{out}\rangle$ lives on the right boundary. We consider an entanglement cut between a subsystem A (of size $\tilde{\ell}$) and its complement $\bar{A}$ (of size $\tilde{L} - \tilde{\ell}$). The depth of the nonunitary circuit is $\tilde{T}$. We also highlight a spacelike surface B along the entanglement cut $t = \tilde{\ell}$. (b) In the limit $\tilde{L} \to \infty$, with $\tilde{\ell}$ finite, system B is isometrically encoded in system $\bar{A}$: For the purpose of computing entropy, the part of the circuit above cut B can be elided. (c) Reduced density matrix on subsystem B. The tracing out of A can be interpreted as the action of decoherence (via a fully depolarizing channel). ρ_B is the output of $\tilde{\ell}$ layers of unitary dynamics *and* decoherence on the edge qudit. (d) Equivalently, one can teleport subsystem A from a timelike surface to a spacelike one by using $\tilde{\ell}$ ancillas (initialized in Bell-pair states) and SWAP gates and compute the entropy of the resulting pure state about the cut between A and B (dashed line).

coupled to a bath that induces decoherence at one of its edges. The main steps in deriving this mapping go as follows (additional technical details are given in Appendix A).

(1) Consider the set of legs denoted by B in Fig. 3(a), which live on a spacelike surface at (unitary) time $t = \tilde{\ell}$. As we show in Appendix A, when $\tilde{L} \to \infty$, the information in B is isometrically encoded in subsystem $\bar{A}$ (the thermodynamically large complement of A) on the right boundary. [83] This means that the information shared between A and $\bar{A}$ is the same as the information shared between A and B; we can, thus, get rid of the entire part of the tensor network above B, reducing the problem to a much smaller circuit of dimensions $\tilde{\ell} \times \tilde{T}$ shown in Fig. 3(b).

(2) Because the state on AB is pure, the entropy of A can be obtained by tracing out either subsystem; we trace out A and obtain the reduced density matrix of B, ρ_B. This amounts to taking two copies of the circuit (a "bra" and a "ket") and connecting them along A. Viewed in the time direction t, after each layer of unitary gates, the rightmost site is traced out and replaced by a maximally mixed state. This corresponds to a fully depolarizing channel [84] acting on the right edge of the system, as illustrated in Fig. 3(c). ρ_B is a mixed state which is the output of this combined unitary-decoherence evolution.

(3) An equivalent picture is obtained by teleporting the right edge of the circuit to a spacelike slice by using ancillas and SWAP gates as discussed earlier. As shown in Fig. 3(d), this gives an enlarged unitary circuit, split in two subsystems A and B where the evolution looks very different (a SWAP circuit on A and the original unitary gates on B).

The upshot is that the spectrum of ρ_A is the same as that of a state ρ_B obtained by evolving the system with $t = \tilde{\ell}$ layers of unitary gates, intercalated by *fully depolarizing noise* at an edge qubit. [85] In formulas,

$$\lim_{\tilde{L} \to \infty} \tilde{S}(\tilde{T}, \tilde{\ell}) = S_{\text{dec}}(t = \tilde{\ell}, L = \tilde{T}), \qquad (1)$$

where we use S_{dec} to denote the entropy of the mixed state evolving with edge decoherence.

First, let us consider the early-time dynamics of the flipped circuit, when $\tilde{T} \ll \tilde{\ell}$. This corresponds to running the boundary-depolarized dynamics for a time that is very long compared to the size of the system ($t = \tilde{\ell} \gg \tilde{T} = L$). As we argue in Appendix A, unless the unitary gates are highly fine-tuned, this dynamics has a unique steady state, which is completely mixed [86]: $\lim_{t \to \infty} S_{\text{dec}}(t, L) = L$. By Eq. (1), this means that, at early times, the entropy of ρ_A grows *ballistically*, at the maximal entanglement velocity allowed by the brick-wall geometry: $\tilde{v}_E = 1$.

The rest of the paper is devoted to understanding what value the entropy saturates to at late times: $\tilde{S}_\infty(\tilde{\ell}) \equiv \lim_{\tilde{T} \to \infty} \lim_{\tilde{L} \to \infty} \tilde{S}(\tilde{T}, \tilde{\ell})$ (in fact, $\tilde{T} > \tilde{\ell}$ is sufficient for saturation). By Eq. (1), this is equal to $S_{\text{dec}}(t = \tilde{\ell})$ in the thermodynamic limit $L \to \infty$. The spatial scaling of late-time entanglement in the flipped circuit is, thus, mapped to the propagation of decoherence from the edge into the bulk of a unitarily evolving system, as a function of time. This is the main result of this section. As it turns out, this is indeed closely related to (but subtly different from) the growth of half-chain entropy in a closed system evolving under the original unitary circuit.

We now provide some intuition on the behavior of $S_{\text{dec}}(t)$ and argue that, at least for chaotic models, it is similar to the growth of entanglement in a *purely unitary* circuit, without edge decoherence. To see why, it is useful

to consider the evolution of the reduced density matrix ρ_B from an operator-spreading perspective [49,50]. In this formulation, one considers expanding the density matrix of the full state in a basis of Pauli strings; the reduced density matrix of B is simply given by those strings that are supported entirely within B. As operators spread out under unitary dynamics, strings that are initially contained in B eventually develop support outside it, increasing the state's entropy. We can now compare two situations: (i) an infinite unitary circuit, with the same type of gates applied everywhere, and (ii) the one depicted in Fig. 3(d), where the gates outside of B are replaced with SWAP gates. Within B, the two are clearly the same. The difference is that, in case (ii), once a Pauli string's end point leaves B, it is "radiated" away by the SWAP gates, with no chance of ever returning. [87] This is in contrast with case (i), where operators have the possibility to shrink and reenter B. Since such shrinking processes are rare—at least for sufficiently chaotic dynamics—we can expect (i) and (ii) to behave similarly.

In summary, we show that, given a unitary circuit U, the entropy of a contiguous region of size $\tilde{\ell}$ in the late-time output state of the (nonunitary) dual circuit $\tilde{U}$ is the same as that of a semi-infinite chain evolving under U *and boundary decoherence* for time $t = \tilde{\ell}$. This latter description is, in turn, related to the growth of half-chain entanglement entropy under unitary dynamics, except that operators that straddle the cut are never allowed to shrink. Since the shrinking of operators is already rare under chaotic dynamics, one might expect this difference to be negligible. We show below that, while this is true to leading order for chaotic dynamics, an important difference nevertheless appears in the form of subleading logarithmic contributions. These can, in turn, become the leading contribution for localized dynamics, where the unitary evolution produces entanglement very slowly or not at all.

Before moving on to applications of this mapping, we note that the above derivation applies to the case when the subsystem A is at the edge of a half-infinite chain. Alternatively, we could consider a situation where the chain is infinite on both sides and A corresponds to a block of sites in its bulk. In that case, the reduction of the circuit—from Fig. 3(a) to Fig. 3(b)—can be done on both sides, both above and below A. The resulting circuit has a less transparent interpretation. [88] Nevertheless, intuitively one expects that the leading-order scaling with $\tilde{\ell}$ should be the same for both physical situations. We confirm this for the Haar-random circuit case in Sec. IV. However, we also find that the coefficient of the aforementioned logarithmic correction is *different* in the two cases, a fact which we explain in terms of properties of random walks.

C. Models of unitary dynamics

To ground our discussion, it is helpful to consider a specific set of experimentally realizable unitary circuit

models that, given appropriate parameter choices, can exhibit all the relevant types of entanglement dynamics. For concreteness, we consider a family of "kicked Ising models": one-dimensional spin chains evolving under the Floquet unitary

$$U_F = e^{-i\sum_n g_n X_n} e^{-i\sum_n h_n Z_n + J_n Z_n Z_{n+1}}, \qquad (2)$$

where the transverse fields g, longitudinal fields h, and Ising couplings J may take any (clean or disordered) values. These models are already at the center of many important developments in quantum dynamics, from out-of-equilibrium phases [4,89] to quantum chaos [60,61,90]. While Eq. (2), as written, is in the form of a time-dependent Hamiltonian, it can be easily recast into a brickwork circuit of two-qubit gates (i.e., it can be "Trotterized" exactly). These models can be realized in Rydberg atoms or digital simulators such as Google's Sycamore processor [91,92]. Spacetime duality then allows us to associate a nonunitary circuit to each such unitary circuit.

The model in Eq. (2) can realize the entire range of entanglement growth regimes summarized in Fig. 1, sorted here from slowest to fastest.

(i) Floquet-Anderson localization, where $S(t)$ saturates to an area law in $O(1)$ time. Achieved by setting $h \equiv 0$ (which makes the model free) and having disorder in J and g.

(ii) MBL, with slow logarithmic entanglement growth, $S(t) \sim \log(t)$. A parameter manifold where the MBL phase in this model has been studied [46] is $g \equiv 0.72\Gamma$, $J \equiv 0.8$, and $h_n \equiv 0.65 + 0.72\sqrt{1 - \Gamma^2} G_n$, where G_n are standard normal variables. The model has an MBL-to-thermal transition at $\Gamma_c \simeq 0.3$.

(iii) Strongly disordered thermalizing dynamics near the MBL transition, where entanglement growth is *sub-ballistic*, $S(t) \sim t^\alpha$ [24]. Realized, e.g., by the above model at $\Gamma \gtrsim 0.3$.

(iv) Dynamics deep in the ergodic phase, where entanglement growth is ballistic, $S(t) \sim v_E t$, with finite "entanglement velocity" v_E [48–50,93–95]. Realized, e.g., by the above model at $\Gamma \simeq 1$.

(v) Dual-unitary dynamics. Realized by setting $g = J = \pi/4$, for arbitrary h_n. This is a provably chaotic model (sometimes called "maximally chaotic") with maximum entanglement velocity [61].

We begin by examining the extremes of this range—localized dynamics in Sec. III and generic chaotic dynamics (including the dual-unitary case) in Sec. IV. We then analyze the sub-ballistic regime in Sec. V. In the latter two cases, rather than trying to simulate the kicked Ising chain directly (which suffers from finite size limitations), our analysis focuses on coarse-grained models with analytic and numerical tractability that are expected to reproduce the same qualitative behavior in the appropriate regimes.

III. LOGARITHMICALLY ENTANGLED STEADY STATES

The discussion in Sec. II highlights a close but subtle relationship between (i) *entanglement growth in unitary circuits* and (ii) *scaling of late-time entanglement* in their spacetime duals. We begin our exploration of this relationship in a class of models where the difference is sharpest: free-fermion Floquet-Anderson-localized circuits where the unitary evolution is periodic in time, noninteracting, and disordered.

In Floquet-Anderson-localized circuits, eigenmodes of the Floquet unitary $\hat{b}_n$ are given by superpositions of on-site fermionic modes $\hat{a}_n$ with exponentially decaying envelopes: $\hat{b}_m \equiv \sum_n \psi_n^{(m)} \hat{a}_n$, $|\psi_n^{(m)}| \sim e^{-|x_m - n|/\xi}$ (ξ is the single-particle localization length, [96] and x_m is the position of the mth orbital's center). Since there are no interactions (and, thus, no dephasing), entanglement growth about a cut originates entirely from orbitals straddling the cut; this leads to saturation to an area law at late times: $S(t) \sim t^0$ for $t \gg 1$. One may expect this behavior to translate to area-law entangled steady states in the spacetime-dual circuit. However, as we show next, entanglement in these models saturates instead to a *logarithmically divergent* value. This provides an example of a more general result—that entanglement *cannot* saturate to an area law in spacetime duals of unitary circuits, except for some trivial fine-tuned exceptions. This is a straightforward consequence of the aforementioned fact that ρ_B [the output of unitary dynamics with edge decoherence, sketched in Fig. 3(c)] eventually has to reach an infinite temperature state, as we prove in Appendix A.

We can obtain the logarithmic scaling of $\tilde{S}_\infty(\tilde{\ell})$ from the mapping in Eq. (1). We, therefore, consider the density matrix ρ_B obtained by evolving a pure initial state with $t \equiv \tilde{\ell}$ layers of the unitary Floquet-Anderson circuit *and* a depolarizing channel on one of the edge sites [as sketched in Fig. 4(a)]. The overall process is a fermionic Gaussian map and can be studied within the free-fermion formalism—one can, in particular, compute its (complex) eigenvalues and eigenmodes and from them compute the entanglement $S_{\text{dec}}(t)$ (note that the initial Bell-pair state is itself Gaussian). Numerical results are shown in Fig. 4(b) for the Ising model (2) in the noninteracting limit $h_n = 0$ ($J_n \equiv \pi/3$ and g_n maximally disordered in $[0, 2\pi]$); they clearly show a logarithmic growth of the average entropy, with single realizations additionally showing an interesting steplike structure.

The result can be understood intuitively as follows. Imagine starting with the purely unitary circuit, with its localized eigenmodes, and continuously switching on the depolarizing noise at the boundary. The orbitals of the unitary model are affected by the noise only to the extent that they overlap with the noisy site, which is an exponentially small effect for orbitals localized far from the
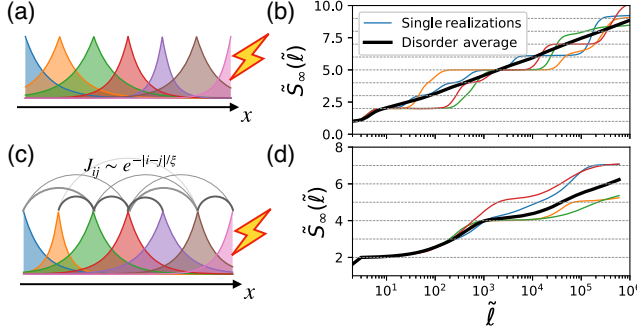
FIG. 4. Logarithmic entanglement in spacetime duals of localized circuits. (a) Schematic of Floquet-Anderson orbitals with edge decoherence. Each exponentially localized orbital decoheres over a timescale τ_n dictated by its overlap with the edge site. (b) Results of numerical fermionic Gaussian state simulations (see details in the main text). The disorder-averaged entropy $\tilde{S}_\infty$ grows logarithmically with $\tilde{\ell}$, while individual realizations show steps associated to the decoherence of individual orbitals. (c) Similar sketch for the Floquet MBL problem; the difference with (a) is that the exponentially localized l-bits τ_i^z interact with each other. (d) Entropy vs subsystem size $\tilde{S}(\tilde{\ell})$ for the dual of the Floquet MBL model at $\Gamma = 0.1$ (see the text). Full density matrix evolution of $\tilde{T} = 9$ qubits evolving under the Floquet MBL circuit with edge decoherence. The behavior is qualitatively similar to that of the Floquet-Anderson problem, with steps and plateaus associated to the depolarization of individual l-bits.

boundary. Therefore, the mth orbital picks up a small imaginary contribution to its energy, of size approximately $e^{-|x_m|/\xi}$, which sets a timescale $\tau_m \sim e^{|x_m|/\xi}$ for the orbital to be decohered by the boundary. At time t, all orbitals with $\tau_m \ll t$ have fully decohered, and each of them contributes one bit of entropy to $\rho(t)$; conversely, orbitals with $\tau_m \gg t$ remain unaffected by the decoherence and contribute no entropy. As a result, we have $S(t) \sim \xi \log(t)$. We conclude that late-time states in the spacetime-dual circuit have entanglement scaling $\tilde{S}_\infty(\tilde{\ell}) \sim \log \tilde{\ell}$, with a nonuniversal coefficient proportional to the localization length ξ in the associated unitary circuit—which, in turn, can be tuned by, e.g., adjusting the disorder strength.

A similar analysis carries over to Floquet MBL systems [44–46,97], with the local integrals of motion (*l-bits*) [47,98] playing the role of Floquet-Anderson orbitals. In particular, it is still true that the l-bits' exponential tails expose them to the effects of edge decoherence; however, in addition, the l-bits can also directly dephase each other due to their (exponentially weak) interactions, potentially accelerating the spread of entanglement in the system [see Fig. 4(c)]. In the unitary circuit, exponentially decaying interactions between the l-bits lead to a characteristic logarithmic growth of entanglement in time [18–20]. When considering the spacetime-dual circuit, there are, therefore, two distinct sources of logarithmic dependence on $\tilde{\ell}$: one from naïvely exchanging space and time and one from the boundary decoherence that causes logarithmic

growth even in the Anderson-localized circuits discussed above. The combination of these two still results in $\tilde{S}_\infty(\tilde{\ell}) \sim \log \tilde{\ell}$, as confirmed numerically by the data shown in Fig. 4(d). Here, we use the version of the Ising model (2) from Ref. [46] (also introduced in Sec. II C), where Γ is used to tune across an MBL-to-thermal transition (at $\Gamma_c \simeq 0.3$); we use $\Gamma = 0.1$, deep in the MBL phase.

We note that, while the steady states discussed in this section exhibit a logarithmic scaling of entanglement, they otherwise do not appear to be "critical" (e.g., the coefficient of the logarithm is fully nonuniversal), and we do not expect them to exhibit conformal symmetry, unlike other recent examples of logarithmic entanglement in nonunitary systems [99,100]. Possible connections between these states and other logarithmically entangled, noncritical states in unitary systems (e.g., at infinite-randomness fixed points [101,102]) are an interesting question for future work.

IV. NONTHERMAL VOLUME-LAW ENTANGLED STEADY STATES

Next, we turn to chaotic unitary dynamics. Such dynamics are fruitfully modeled by random circuits where each two-site gate is an independently chosen Haar-random unitary. As minimal models for chaotic quantum evolution, these circuits have been studied extensively and are known to capture various universal features of operator spreading and entanglement growth [93–95,103–106]. Here, we make use of these results to uncover universal features of steady states of spacetime duals of chaotic unitary evolutions, such as the clean limit of the kicked Ising chain (2).

The quantity that lends itself to a particularly simple calculation in the Haar-random circuit is the so-called *annealed average* of the second Rényi entropy, which is obtained by averaging the purity of a subsystem over realizations of the random circuit and then taking a logarithm [107]: $q^{-S_2^{(a)}(t)} \equiv \overline{\mathcal{P}_A(t)}$, where the purity of the reduced density matrix ρ_A is defined as $\mathcal{P}_A = \text{Tr}(\rho_A^2)$ and the overline denotes averages over circuit realizations. It is known that this quantity can be evaluated in terms of a classical random walk for the end point of a domain wall-like object which we define below [94]. In our case, the boundary depolarization changes this calculation by inducing a partially absorbing boundary condition on this random walk. As a result, the purity picks up an additional factor proportional to approximately $t^{-1/2}$ (the survival probability of the random walk). Upon taking the logarithm, this gives the result

$$\tilde{S}_{2,\infty}^{(a)}(\tilde{\ell}) = S_{2,\text{dec}}^{(a)}(t = \tilde{\ell}) = v_E \tilde{\ell} + \frac{1}{2} \log \tilde{\ell} + \cdots, \quad (3)$$

where $\cdots$ stands for corrections that are at most constant in $\tilde{\ell}$. Note that the entropy density exactly coincides with the entanglement velocity in the unitary circuit, v_E. Moreover, there is a subleading logarithmic correction
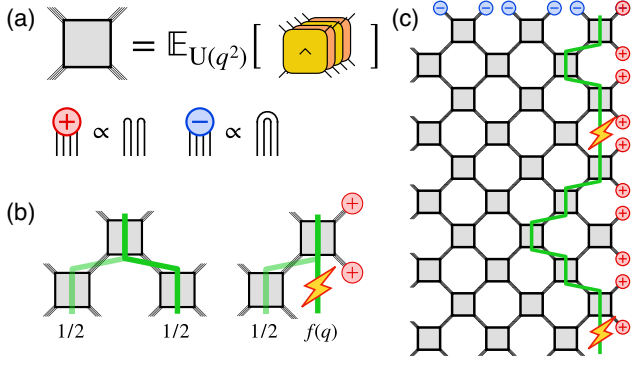
FIG. 5. Random-walk calculation of average purity in Haar-random circuit with boundary decoherence. (a) Notations: The gray boxes represent Haar-averaged unitary gates; the $\pm$ symbols represent the two ways of pairing up the four legs; the purity calculation involves a domain wall between $-$ and $+$. (b) Elementary steps of the random walk in the bulk (left) and boundary (right), where probability is not conserved [$f(q) < 1/2$]. (c) A realization of the random walk. Whenever the random walker hits the boundary, its survival probability decreases (lightning symbols).

whose $1/2$ prefactor is fixed by the diffusive dynamics of the entanglement domain wall.

In order to derive Eq. (3), let us first briefly review how the calculation of $\overline{\mathcal{P}_A(t)}$ proceeds in the original Haar-random unitary circuit. Since $\mathcal{P}_A$ is quadratic in the density matrix, this calculation involves *four* copies of the circuit: two ket and two bra variables for each leg. To get a nonzero average, one needs to pair ket and bra variables, which can be done in two inequivalent ways, denoted by $+$ and $-$ in Fig. 5(a). Averaging each gate over the Haar measure results in a two-dimensional tensor network that can be thought of as an Ising-like classical partition function in terms of the $\pm$ variables. On the lower boundary of this tensor network, the boundary conditions are fixed by the initial state $|\psi_0\rangle$, while on the upper boundary one should have a domain of $-$ states inside A surrounded by $+$ states in its complement.

Let us focus on the case when the subsystem A is half of an infinite chain. In this case, the boundary condition takes the form of a domain wall in the Ising formulation. One can then consider evaluating the full 2D tensor network row by row, starting from this boundary state. The great simplification arising from Haar averaging is that, at each step, the domain wall evolves into similar domain-wall configurations; when a gate is applied at the position of the domain wall, its end point moves randomly left or right with equal probabilities while picking up an overall prefactor. This corresponds to a recursion relation of the purities which takes the form

$$\mathcal{P}(x,t) = \frac{2q}{q^2+1} \frac{\mathcal{P}(x-1, t-1) + \mathcal{P}(x+1, t-1)}{2}, \quad (4)$$

whenever a gate is applied on the bond between sites x and $x+1$. Here, we use $\mathcal{P}(x,t)$ to denote the purity of the subsystem $A = [-\infty, \ldots, x]$ at time t. Following this process all the way back to time 0, we end up with the result

$$\mathcal{P}(x,t) = \left(\frac{2q}{q^2+1}\right)^t \sum_y K_{xy}(t) \mathcal{P}(y,0), \quad (5)$$

where $K_{xy}(t)$ is the propagator (from position x to y) of a simple random walk. For a product initial state [108], we have $\mathcal{P}(y,0) = 1$ for all y. By normalization, we also have $\sum_y K_{xy}(t) = 1$ at all times. Therefore, we end up with a simple result: $\mathcal{P}(x,t) = q^{-v_E(q)t}$, where $v_E(q) = \log[(q+q^{-1})/2]$ is the *entanglement velocity* [109].

How does this result change when we take the spacetime dual of the Haar-random circuit or, equivalently, when we add depolarizing noise at the right boundary? Inside subsystem B, the domain wall performs the same random walk as before. However, when it hits the boundary of B, the depolarizing channel imposes *partially absorbing* [112] (also known as *radiation*) boundary conditions on it. Whenever the domain wall would leave B, it instead remains on the same position but picks up an extra factor of $1/q$. Whenever this happens, the domain wall is "out of sync" with the circuit and misses the following layer of gates. This results in an additional factor of q^{v_E}. Overall, this means that whenever the domain wall hits the boundary, it picks up a factor of $2f(q) \equiv q^{v_E-1} < 1$, decreasing its total survival probability. This is illustrated in Figs. 5(b) and 5(c).

Applying this logic, we find that the purity of the evolution with boundary depolarization becomes

$$\tilde{\mathcal{P}}(x,t) = q^{-v_E(q)t} \sum_y \tilde{K}_{xy}(t) \tilde{\mathcal{P}}(y,0), \quad (6)$$

where $\tilde{K}_{xy}(t)$ is now the propagator for the random walk with a partially absorbing boundary at $x = \tilde{T}$. We are considering cases where $\tilde{\mathcal{P}}(y,0)$ is independent of y, so overall the purity picks up a multiplicative factor proportional to the total survival probability of the random walk. At long times, this scales as the return probability of the random walk on an infinite chain [113], resulting in $\tilde{\mathcal{P}}(x,t) \propto q^{-v_E(q)t}/\sqrt{t}$. We also provide independent confirmation of this result through large-scale simulations of random Clifford circuits (which exactly agree with the Haar-random circuit for the purity calculation), whose results are shown in Fig. 6. Details on the method, as well as results on other interesting properties of this nonthermal volume-law entangled phase (from the point of view of dynamical purification [8]), are discussed in Appendix B.

For the entropy calculation in the spacetime-dual circuit, the relevant initial condition is one in which the domain wall sits right at the boundary, $x = \tilde{T}$ [Fig. 5(c)]. The purity
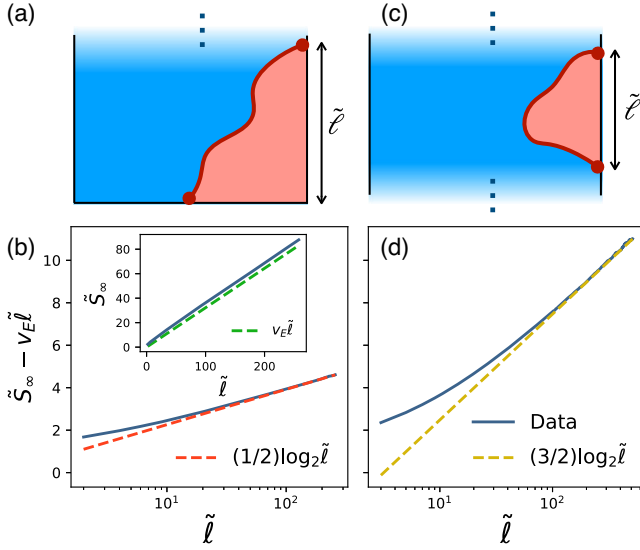
FIG. 6. Entanglement entropy in spacetime duals of Haar-random circuits. (a) Schematic of a finite subsystem at the edge of a semi-infinite system: The entropy calculation maps to random-walk survival probability (the starting point is pinned to the entanglement cut; the end point is free). (b) Numerical results for the entropy confirm the analytical prediction: a volume-law term $v_E \tilde{\ell}$ [inset; $v_E = \log_2(5/4)$] with a $(1/2) \log \tilde{\ell}$ nonthermal correction. (c) Schematic of a finite subsystem in the bulk of an infinite system: Entropy calculation maps to random-walk return probability (starting and ending points are pinned to the edges of the subsystem). (d) Numerical results agree with the predicted $(3/2) \log \tilde{\ell}$ correction. Numerical data in (b) and (d) are from stabilizer simulations of Clifford unitary circuits with edge decoherence with $\tilde{T} = 129$ qubits; the annealed average is over 10^6 circuit realizations. For (d), the initial mixed state [bottom in (c)] is implemented by adding $\tilde{T}$ reference qubits with no dynamics.

at time t then becomes the purity of a subsystem in the long-time steady state with length $\tilde{\ell} = t$. Putting this all together, we find Eq. (3). There are two noteworthy features of this result. First, the steady state exhibits volume-law entanglement, with a density $\lim_{\tilde{\ell} \to \infty} (\tilde{S}_{2,\infty}^{(a)}/\tilde{\ell})$ equal to the speed of entanglement growth in the unitary dynamics, $v_E(q)$. Second, there is a subleading contribution $(1/2) \log \tilde{\ell}$ that arises due to the boundary decoherence and is *absent* in the original unitary circuit. In this sense, the long-time steady state is *nonthermal*, despite its volume-law entanglement.

As we note, the $1/2$ coefficient of the logarithmic correction has its origins in the survival probability of the random walker decaying as $t^{-1/2}$. This is the appropriate quantity to calculate in the situation we have been considering so far, where the subsystem A lives at the edge of the 1D chain [see Fig. 3(a)]; this means that the domain wall has no preference on where to end up as long as it stays in the system. The calculation changes if we instead consider a subsystem in the bulk of an infinite chain.

In that case, the boundary conditions in Fig. 5(c) need to be changed: We need to enforce the same domain wall configuration at both the initial and the final time on the partition function. This means that, instead of the survival probability, we need to consider the *return probability*. [114] This instead decays as $t^{-3/2}$, giving rise to a correction $(3/2) \log \tilde{\ell}$ in the entropy.

We expect the prefactors ($3/2$ in the bulk and $1/2$ at the edge) to be universal for spacetime duals of chaotic unitary circuits. As can be seen from the above derivation, the origin of this prefactor lies in the diffusive dynamics of the purity domain wall. This description, in terms of a diffusing domain wall, is expected to apply for generic (space- and time-translation invariant) chaotic unitary circuits in the long-time, large-distance limit (it is an emergent description on par with the usual diffusion of conserved quantities) [115,116]. For this reason, our derivation above should also capture the universal features of spacetime duals of such chaotic circuits. The situation becomes more complicated for circuits that possess continuous symmetries. However, a similar description in terms of a diffusing domain wall exists even for these [106], and, therefore, we conjecture that they would also exhibit the same $(3/2) \log \tilde{\ell}$ contribution. In fact, this term is exactly the same as the one conjectured to arise in hybrid (unitary-measurement) circuits [6,42,43] in their volume-law phase; indeed, one could think of the domain wall picture we describe as a microscopic realization of the "directed polymer in a random environment" (DPRE) effective description in Ref. [117]. This is further supported by a diagnostic discussed in Appendix C, based on the scaling of mutual information between a single qubit and an extensive subsystem separated by a distance x. We find that this diagnostic scales as approximately $x^{-1.2}$ for duals of unitary circuits, in complete agreement with its behavior in generic hybrid circuits and the DPRE effective theory. These findings strongly suggest that duals of chaotic circuits realize the same nonthermal volume-law phase as generic monitored circuits. Given the superior analytical tractability of duals of unitary circuits, this analysis opens new routes for the study of this phase and its properties as an emergent error-correcting code [43], which is an interesting direction for future research.

A notable exception to the universality of logarithmic corrections in duals of chaotic circuits is provided by dual-unitary circuits: In this case, the flipped circuit is itself unitary and, thus, heats up to an infinite temperature state rather than reaching nonthermal steady states of the kind realized by generic circuits; in particular, since the entropy is already maximal, there is no place for a logarithmic correction (negative log corrections are disallowed by subadditivity of the entropy). This can be understood from the operator-spreading perspective discussed in Sec. II B. Dual unitarity ensures [62,64,65] that operator strings always grow at the maximal possible speed. Consequently, there are

no "shrinking" processes that could be killed by the boundary decoherence, and the steady-state entanglement in the flipped direction is exactly equivalent to growth of entanglement in the unitary time direction: $\tilde{S}_\infty(\tilde{\ell}) = \tilde{\ell} = t$.

Finally, we need to comment on the issue of the order of averages in the Haar-random circuit. In the above, we focus on the annealed average, wherein we average the purity over circuit realizations before taking its logarithm. The quenched average, i.e., the average of S_2 itself, has a more complicated dynamics, described by the Kardar-Parisi-Zhang (KPZ) equation [93,111]. Among other things, this leads to a universal subleading contribution to the entropy growth in the unitary circuit of the form $at^{1/3}$ (where the constant a itself is nonuniversal). We expect that, upon flipping the circuit, this would lead to a contribution $a\tilde{\ell}^{1/3}$ in the quenched average of the entropy for the steady state, in agreement with recent results on random monitored Clifford circuits [117]. However, since the KPZ equation can be equivalently formulated in terms of multiple interacting random walkers, each of which would feel the same partially absorbing boundary, we conjecture that the overall result takes the form

$$\overline{\tilde{S}_2}(\tilde{\ell}) = v_E^{(q)}\tilde{\ell} + a\tilde{\ell}^{1/3} + \frac{1}{2}\log\tilde{\ell} + \text{const} + \cdots,$$

where we use $v_E^{(q)}$ to denote the speed associated to the quenched average of the entropy, which can be different from the one we calculate above for the annealed average. Note that the $t^{1/3}$ contribution is a result of spacetime randomness in the Haar circuit. As such, we expect the corresponding $\tilde{\ell}^{1/3}$ to be present in the spacetime duals of such random circuits but to be absent for ones that are periodic in time.

V. FRACTALLY ENTANGLED STEADY STATES

A. Griffiths circuit model

Having examined the two extremes of dynamics in localized systems (Sec. III) and in chaotic ones (Sec. IV), we now turn to slowly thermalizing dynamics in disordered systems, for instance, near an MBL transition on the thermal side. There, entanglement growth is thought to be sub-ballistic, $S(t) \sim t^\alpha$, $0 < \alpha < 1$, due to the impact of Griffiths effects—rare localized regions which serve as bottlenecks to the dynamics [21–25,118–121]. As both the localized and chaotic cases reveal a close relationship between $S(t)$ (entanglement growth in unitary circuits), on the one hand, and $\tilde{S}_\infty(\tilde{\ell})$ (scaling in space of the late-time entanglement in the dual circuit), on the other, the sub-ballistic growth of $S(t)$ in these "thermalizing Griffiths models" suggests the intriguing possibility of producing late-time states with fractal entanglement scaling, $\tilde{S}_\infty \sim \tilde{\ell}^\alpha$ with a tunable $\alpha \in (0,1)$.
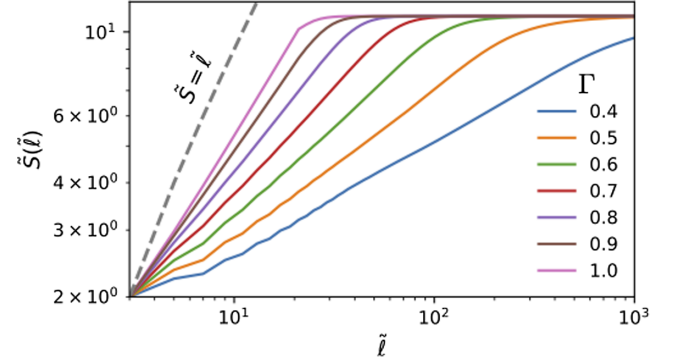

FIG. 7. Entropy $\tilde{S}_\infty$ for the spacetime dual of the kicked Ising circuit Eq. (2) in the ergodic phase, at depth $\tilde{T} = 11$ (numerical data from exact density matrix evolution for unitary evolution with edge decoherence). The parameter Γ controls the relative strength of disorder; the model has a thermal-to-MBL transition at $\Gamma_c \simeq 0.3$.

We see indications of this behavior in the kicked Ising model in Eq. (2), studied in the parameter regime in Ref. [46] (also summarized in Secs. II C and III) which features a transition from an MBL phase to a thermal one. As discussed in Sec. II C, this model has a parameter $\Gamma \in [0,1]$ which sets the disorder strength $W \propto \sqrt{1-\Gamma^2}$ and tunes across an MBL-to-thermal transition at $\Gamma_c \simeq 0.3$. Exact density matrix simulations for the unitary circuit with edge decoherence, whose results are shown in Fig. 7, display a range of power-law exponents that decrease closer to the MBL transition ($\Gamma_c \simeq 0.3$). However, the computational method limits us to modest depths $\tilde{T} \approx 10$, which, in turn, limits the available dynamic range and makes it difficult to characterize the fractal scaling. Likewise, the properties of the dual transition between logarithmic and fractal scaling of steady states are severely finite-size impacted.

For this reason, we turn to a more fruitful approach that relies on random circuits to capture coarse-grained features of the underlying sub-ballistic dynamics. Here, we use a family of models introduced in Ref. [25], consisting of random circuits on one-dimensional spin chains where every bond x is assigned a distinct rate γ_x, meant to capture the rate of entanglement propagation through a large disordered region in a coarse-grained way. The rates are independently and identically sampled from a distribution $P(\gamma) = (a+1)\gamma^a$, $\gamma \in [0,1]$, where the parameter $a \in (-1,+\infty)$ effectively controls the strength of disorder—the smaller a, the more $P(\gamma)$ is concentrated near $\gamma = 0$, the more "weak links" in the chain. Once rates $\{\gamma_x\}$ for all bonds are chosen, the system evolves via a spatiotemporally random circuit where each bond is acted upon by a gate every approximately γ_x^{-1} time steps. Concretely, we use a brickwork circuit structure where each gate on bond x is either 1 (with probability $1-\gamma_x$) or a Haar-random gate (with probability γ_x); see Fig. 8(a). In this model,
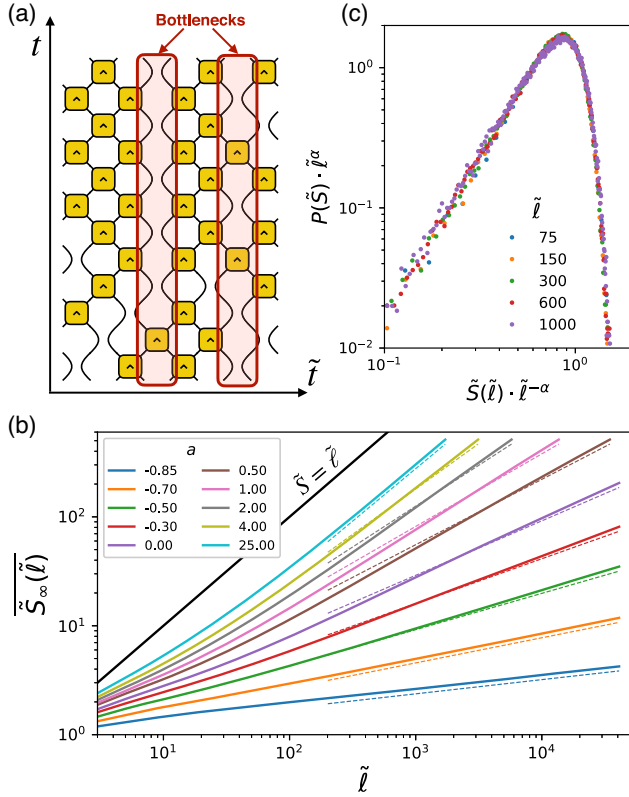
FIG. 8. Fractal entanglement from the Griffiths circuit model. (a) Schematic of the circuit: Each bond x is assigned a rate γ_x that sets how often unitary gates act there; bonds where $\gamma_x \ll 1$ act as bottlenecks for the spread of entanglement (highlighted). Under spacetime duality, bottlenecks correspond to catastrophic events, where simultaneous Bell measurements are performed on most qudit pairs. (b) Average entanglement entropy $\overline{\tilde{S}(\tilde{\ell})}$ in late-time output states of a version of this circuit where nonidentity gates are drawn from the two-site Clifford group (using $\tilde{T} = 1024$ qubits and averaging over 10^5 disorder realizations). By varying the effective disorder strength a, $\overline{\tilde{S}}$ can be made to scale as $\tilde{\ell}^\alpha$ with any power-law exponent $0 < \alpha < 1$. The black line represents the maximal entropy $\tilde{S} = \tilde{\ell}$; dashed lines represent the predicted power-law scaling $\alpha = (a+1)/(a+2)$. The disagreement for intermediate a is due to subleading corrections (see Appendix D). (c) The entire distribution of $\tilde{S}$ (not just its mean) shows a scaling collapse, $P(\tilde{S}) \sim \tilde{\ell}^{-\alpha} P(\tilde{S}/\tilde{\ell}^\alpha)$ (data for $a = 1$, fit exponent $\alpha = 0.73$ vs predicted $2/3$).

entanglement grows *sub-ballistically* as $S(t) \sim t^\alpha$, with $\alpha = (a+1)/(a+2) \in (0,1)$ [25].

Under spacetime duality, the disordered rates are not assigned to bonds in the chain but rather to *time steps*, thus creating "temporal weak links" in the evolution. At such a temporal weak link $\tilde{t}$, where $\gamma_{\tilde{t}} \ll 1$, the vast majority of bonds are acted upon by the spacetime dual of the identity, $\tilde{\mathbb{1}} \propto |B^+\rangle\langle B^+|$—i.e., they are projected onto Bell states. This results in a "catastrophic" event where most of the system becomes disentangled, leaving behind a sparse network of unmeasured entangled sites. The repetition of

these events over all scales (in time $\tilde{t}$ and rate γ) prevents entanglement from ever saturating to a volume law and instead gives rise to a fractal pattern of entanglement in late-time states.

B. Fractal entanglement

This result is straightforwardly proved in the edge decoherence picture by adapting the discussion in Ref. [25], with minor changes from the closed-system case to the edge-decoherence one. First, imagine a situation where the rates are uniform, $\gamma_x \equiv \gamma^{(0)}$, except for a single "weak link" at a distance x_1 from the decohering edge, where the rate is $\gamma_{x_1} \equiv \gamma^{(1)} \ll \gamma^{(0)}$. At early times, the depolarizing noise quickly decoheres the region between the weak link and the boundary, giving a ballistic growth $S(t) \sim \gamma t$ similar to the Haar-random case discussed in Sec. IV. At later times, the bottleneck at x_1 sets the rate of entropy growth, [122] while the region between the weak link and the boundary essentially saturates to a fully mixed state, resulting in $S(t) = \min\{\gamma^{(0)}t, x_1 + \gamma^{(1)}t\}$. Generalizing this argument to the case with a hierarchy of (increasingly far, increasingly weak) links at distances x_n (with $x_0 = 0$) and rates $\gamma^{(n)}$ gives

$$S(t) = \min_n \{x_n + \gamma^{(n)}t\}.$$

In other words, at any given timescale t, there is one "dominant" bottleneck (the value of n minimizing the argument) that is mainly responsible for slowing down the spreading of decoherence through the system. Now, given a length scale ζ, the typical value of the slowest rate encountered within that length scale is [25] $\gamma_{\min}^{(\text{typ})}(\zeta) \sim \zeta^{-1/(a+1)}$. Therefore, we conclude that, typically,

$$S(t) \sim \min_\zeta \{\zeta + \zeta^{-1/(a+1)}t\} \sim t^\alpha, \qquad \alpha = \frac{a+1}{a+2}, \quad (7)$$

i.e., the same sub-ballistic scaling as in Ref. [25]. We emphasize that this is the leading-order scaling, and we do not focus on subleading corrections at this level.

We confirm this result with numerical simulations, using two methods: (i) stabilizer numerical simulations, where the nonidentity gates are sampled uniformly from the Clifford group on qubits ($q = 2$), and (ii) a recursive (random walk) construction like the one used in Sec. IV but adapted to the presence of random rates as detailed in Appendix D. In both cases, we simulate unitary dynamics with edge decoherence. The results of both methods confirm the unconventional scaling of the averaged entanglement entropy with subsystem size, $\tilde{S}_\infty \sim \tilde{\ell}^\alpha$ with fractional exponents $0 < \alpha < 1$; we show this in Fig. 8(b) for the Clifford simulations and in Appendix D for the random-walk method. Small numerical discrepancies between the exponent predicted by Eq. (7) and the data (most evident at

intermediate a) arise from large subleading corrections to scaling, which are expected to be present already in the unitary case, as we discuss in Appendix D. Beyond the fractional power-law scaling of the mean entropy, we find that all moments of the entropy distribution scale in the same way, as manifested by the collapse of the probability distribution $P(\tilde{S}_\infty)$ onto a scaling ansatz $P(\tilde{S}_\infty) \propto \tilde{\ell}^{-\alpha} f(\tilde{S}_\infty / \tilde{\ell}^\alpha)$, shown in Fig. 8(c). This means that the spatial entanglement profile of a typical state drawn from this ensemble appears *statistically self-similar* over all length scales, justifying the "fractal" label. This is in contrast with, e.g., the volume-law phase in Sec. IV where one expects (under quenched averaging) $\bar{S} \sim \ell$ and $\delta S \sim \ell^{1/3}$ (owing to the conjectured KPZ scaling): The relative size of fluctuations in this case is scale dependent and not self-similar.

Another intriguing aspect of these models is studied in Appendix B, where we show data on their purification dynamics [8]. We find that they realize a family of novel *critical purification phases* with a continuously variable dynamical exponent. In particular, the entropy of a maximally mixed initial state decays as $\tilde{S} \sim \tilde{L}/\tilde{t}^{1/z_p}$, with $z_p = a + 1$, and at late time crosses over to an exponential decay (also as a function of the ratio $\tilde{t}/\tilde{L}^{z_p}$), suggestive of CFT behavior [27].

The $\tilde{\ell}^\alpha$ scaling derived above captures the leading-order behavior in this model. Even in the unitary case, there are subleading corrections, as we note above. In the spacetime-dual circuit, we expect that further logarithmic corrections should appear due to the edge decoherence, just as they do in both the localized and chaotic models studied in Secs. III and IV. The most straightforward argument for these comes from generalizing the random-walk calculation in Sec. IV to the present model. In this modified random walk, we now have locations in the circuit where the Haar-random gate is replaced by the identity: These have no effect on the "purity domain wall," while the partially absorbing boundary condition is unchanged. Therefore, the purity should again pick up a power-law decaying contribution from the survival or return probability of the random walker (depending on whether we are considering a subsystem near the edge or in the bulk). However, the power of the decay might be different from the ones derived in Sec. IV. In that case, the end point of the domain wall has diffusive dynamics, a fact that is closely related to the diffusive broadening of operator wavefronts [94]. This latter feature is also expected to change in the Griffiths phase, with a separate, continuously changing "front broadening exponent" at strong enough disorder [25]. Consequently, we expect that the prefactor of the logarithmic correction to the entropy also becomes a continuously varying parameter deep in the Griffiths regime.

C. Robustness to breaking of unitarity

We derive these fractally entangled phases by dualizing unitary circuits U with sub-ballistic entanglement growth.

It is natural to ask whether or not this duality is a necessary condition, i.e., how robust these phases are to perturbing the "original" circuit U away from unitarity. As we show, area-law phases are generically ruled out in nonunitary circuits whose dual is unitary; but, upon lifting this constraint, area-law phases are expected to appear again when a (suitably defined) "measurement rate" is high enough. Do fractally entangled phases survive then, at least in parts of parameter space for sufficiently weak perturbations? Or are they immediately wiped out when unitarity of U is broken?

To address this question, we perturb the unitary "Griffiths circuit" in Fig. 8(a) away from unitarity and study the effect of this perturbation on entanglement in the dual circuit. Concretely, we consider a unitary-measurement circuit with random unitary gates and two-qubit Bell measurements, where the measurement rate is time dependent: $p(t) \equiv 1 - \gamma_t$, with γ sampled from $P(\gamma) = (a+1)\gamma^a$ independently at each time step. This circuit is generally nonunitary in both time directions. However, when the gates are restricted to be dual unitary, this circuit becomes unitary in the space direction: Namely, it is dual to a unitary "Griffiths circuit" as in Fig. 8, where all the nonidentity gates are dual unitary. It is possible to interpolate smoothly between the two cases (fully generic vs dual-unitary gates) by tuning the distance of the gate set from dual unitarity. This is particularly straightforward for the two-qubit Clifford group, which is discrete and such that exactly half of the elements are dual unitary. Sampling preferentially from the dual-unitary half of the group, say, with probability $1 - \delta$, gives a parameter δ that quantifies the breaking of unitarity in the space direction. Do the fractal phases we find at $\delta = 0$ survive to finite $\delta > 0$?

The steady-state entanglement in this family of unitary-measurement circuits, shown in Fig. 9(a) for $\delta = 1/2$ (i.e., uniform sampling of Clifford gates), reveals an interesting picture. As anticipated, an area-law phase appears: The average rate of measurements in this circuit is $\bar{p} = 1 - \bar{\gamma} = [1/(a+2)]$, which becomes large at small a (going to 1 as $a \to -1$); absent obstructions, this is expected to lead to an area-law phase. Indeed, that is what we see for $a \lesssim 0$. However, upon increasing a, the system transitions out of the area-law phase and into a family of fractally entangled phases. We verify that for $a \geq 2$ the scaling is consistent with the expected one: $S(\ell) \sim \ell^\alpha$, $\alpha = [(a+1)/(a+2)]$ [dashed lines in Fig. 9(a)]. At intermediate a, the data are suggestive of a logarithmically entangled critical point (at $a_c \approx 0.5$) that gives way to fractal entanglement with exponent $\alpha(a)$ continuously varying from $\alpha(a_c) = 0$ to $\alpha(a) \simeq [(a+1)/(a+2)]$ at large a. While a detailed study of this transition is left for future research, it is clear that fractal entanglement does indeed survive in a large part of parameter space, even when the original circuit U is strongly perturbed away from unitarity.

A conjectured sketch of the phase diagram as a function of the "bottleneck parameter" a and the unitarity-breaking
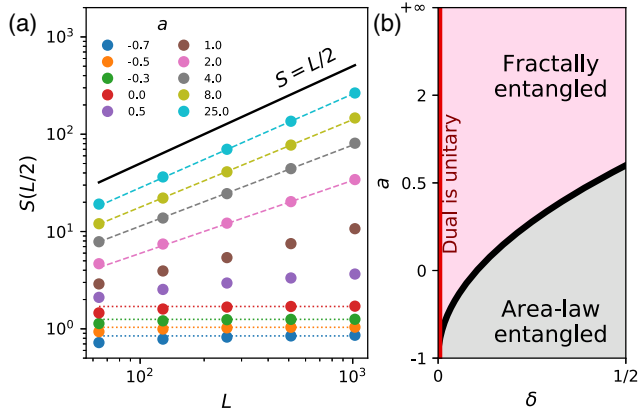
FIG. 9. Robustness of fractal entanglement in $\tilde{U}$ to the breaking of unitarity in U. (a) Half-cut entanglement entropy $S(L/2)$ for a pure state evolving under random Clifford gates and Bell measurements; the measurement probability $1 - \gamma_t$ depends randomly on time, with γ drawn from $P(\gamma) \propto \gamma^a$ independently at each time step. Data from stabilizer simulations, with $L < T < 2L$, averaged over between 10^4 and 5×10^5 realizations depending on size. The system enters an area-law phase for $a \lesssim 0$ (dotted lines are constants), while fractal entanglement persists at $a \gtrsim 1$ [dashed lines have slope $\alpha \equiv (a+1)/(a+2)$]. (b) Sketch of conjectured phase diagram as a function of the bottleneck parameter a and the deviation from unitarity δ [see the text; (a) corresponds to $\delta = 1/2$]. The $\delta = 0$ line corresponds to the circuit U being unitary, which forbids the area-law phase in $\tilde{U}$.

perturbation strength δ is shown in Fig. 9(b). The area-law phase in $\tilde{U}$ appears continuously as the circuit U is detuned from unitarity, while the phases identified at $\delta = 0$ survive in part of parameter space. We conjecture that this behavior is generic—i.e., that all the entanglement phases identified in this work should be robust to weak breaking of unitarity in the transverse direction.

VI. SUMMARY AND OUTLOOK

In this work, we have explored entanglement in non-unitary circuits that are spacetime duals of local unitary circuits [30]. Focusing on this class of nonunitary circuits has allowed us to translate the rich variety in entanglement growth displayed by unitary circuits into an equally rich variety of steady-state phases produced by nonunitary dynamics. Most notably, these include a large and robust family of *fractally entangled* late-time states, whose entanglement evades the usual categories of volume-, area-, or log-law that cover nearly the entirety of eigenstates or steady states encountered in unitary dynamics.

Another important advantage of these circuits lies in their analytical tractability: Ideas and methods developed for unitary dynamics can be borrowed and used to great effect, providing an analytical handle on nonunitary dynamics away from well-understood limits (e.g., large local Hilbert space, etc.). In particular, we have derived a general identity relating steady-state entanglement in these

nonunitary circuits to the entropy of mixed states evolving through a combination of unitary dynamics and decoherence. This powerful mapping has allowed us to identify and characterize logarithmic corrections to entanglement in various regimes: In the duals of chaotic circuits, these corrections sharply distinguish the volume-law entangled phase from a thermal one (while possibly placing it in the same universality as the nonthermal volume-law phase in weakly monitored circuits); in the duals of localized circuits, these corrections can even become the *leading* contributions, essentially ruling out area-law entangled phases.

We also detailed how these novel steady states can be prepared experimentally on near-term quantum simulators, with an experimental protocol based on quantum teleportation that relies on ordinary unitary evolution and a *vanishing density* of postselected measurements in spacetime (as opposed to the finite density that characterizes generic unitary-measurement circuits). Lowering the required number of measurements has important implications for the practicality of reliably preparing these states without the use of auxiliary classical simulation.

Our work raises several intriguing questions for future research. Understanding more about the nature of the fractally entangled steady states we found in the duals of thermalizing Griffiths phases, and what other contexts they might occur in, is an exciting goal for future research. It is particularly intriguing to speculate about the possibility of realizing these unconventional states (which are natively the output of $1 + 1$-dimensional nonunitary circuits) as ground states of generalized (possibly non-Hermitian) Hamiltonians and study the role of symmetry therein [123].

Another interesting open question is the precise nature of the volume-law phase we identified in the spacetime duals of generic clean (or weakly disordered) unitary circuits. As we noted, the universal prefactor of the logarithmic correction agrees with what is expected in weakly monitored unitary circuits. Another diagnostic based on mutual information (analyzed in Appendix C) does not conclusively discriminate the two phases, either. This leaves two interesting possibilities: (i) that the duals of chaotic unitary circuits realize a novel nonthermal volume-law entangled phase or (ii) that they provide an exact realization of the same phase in a way that is substantially more tractable in theory and more accessible in experiment. Determining which of these two scenarios is realized is an exciting question for future research.

More generally, it would be interesting to build a more complete understanding of these nonthermal states and the place they occupy in the broader landscape of dynamical many-body states, e.g., through the lens of chaos, complexity, and thermalization. ("Nonthermal" is, after all, a rather vague label.) It would also be interesting to study the properties of nonunitary phase transitions dual to unitary transitions; the Floquet Ising model studied here does have a (unitary) transition between MBL and thermalizing phases, but the properties of its dual nonunitary counterpart

were challenging to study due to the limitations of finite system size numerics.

In this work, we have mainly focused on quantum entanglement; however, characterizing these novel steady states from the standpoint of quantum order is another natural direction for future research. Can these states host nonequilibrium ordered phases? In most known cases in the unitary domain, out-of-equilibrium phases rely on MBL and *eigenstate order* [89,124]; how does the impossibility of area-law states in these spacetime-dual circuits affect the definition of phases? And how are the (leading or subleading) logarithmic corrections manifested in correlation functions? Extending these ideas to higher dimension may also open up exciting directions in relation to topology, e.g., by considering the spacetime duals of $2 + 1$-dimensional Floquet topological phases [125].

Looking ahead, perhaps the most exciting challenge is to push the "nonunitary frontier" by identifying other interesting (and experimentally relevant) corners of nonunitary evolutions that may further reveal new phenomena and broaden our understanding of quantum dynamics.

Note added.—Recently, we became aware of related work [126] which also considers entanglement dynamics in spacetime duals of unitary circuits. Our results agree where they overlap, but our works are largely complementary.

APPENDIX A: DETAILS ON EDGE DECOHERENCE

Here, we clarify some technical details on the mapping to edge decoherence introduced in Sec. II and some results

that follow from it. We argue that, taking the limit $\tilde{L} \to \infty$ with $\tilde{\ell}$ finite (i.e., when A is a finite subsystem of a semi-infinite chain), the entire $\bar{A}$ section of the circuit in Fig. 3(a) can be elided (for the purpose of computing the entropy of A), and it suffices to consider the mixed state ρ_B produced at the spacelike cut B between the timelike surfaces A and $\bar{A}$. Here, we unravel the argument in more detail and in the process clarify how big $\tilde{L}$ needs to be in various models and what the fine-tuned exceptions to this result look like. Finally, as a corollary, we show that area-law entangled steady states are impossible (again up to trivial, fine-tuned exceptions).

1. Uniqueness of the steady state under edge decoherence

To begin, we consider the layout in Fig. 3(c)—unitary evolution with edge decoherence, for a variable time t (also identified with subsystem size $\tilde{\ell}$ in the "flipped" circuit). Let $\rho_B(t)$ be the mixed state produced by t layers of unitary gates accompanied by an erasure channel on the last qubit:

$$\rho_B(t) \equiv \Phi_{\text{edge}} \circ \mathcal{U}_t \circ \Phi_{\text{edge}} \circ \cdots \mathcal{U}_1[\rho_B(0)], \qquad \text{(A1)}$$

where $\mathcal{U}_\tau[\rho] \equiv U_\tau \rho U_\tau^\dagger$ describes the application of one layer of unitary gates at time τ (we do not assume a Floquet circuit) and $\Phi_{\text{edge}}[\rho] \equiv \text{Tr}_{\text{edge}}(\rho) \otimes \mathbb{1}_{\text{edge}}/q$ is the erasure (or fully depolarizing) channel acting on the edge qubit. We prove the following statement: Up to fine-tuned exceptions in the circuit choice $\mathcal{U}_\tau$, the quantum channel Eq. (A1) maps all input states to the maximally mixed state $\rho_B \equiv \mathbb{1}^{\otimes L}/q^L$ as $t \to \infty$.

The proof can be succinctly stated in the operator-spreading language. First, let us consider time-periodic dynamics, $\mathcal{U}_\tau = \mathcal{U}$. We imagine expanding our prospective steady state ρ_∞ in a basis of Pauli strings. Φ_{edge} is a projector onto the subspace spanned by strings that act as the identity on the edge site. Clearly, ρ_∞ must belong to this subspace: $\Phi_{\text{edge}}[\rho_\infty] = \rho_\infty$. Moreover, it also cannot develop any component on the orthogonal subspace (i.e., the space of operators that do *not* act as the identity on the edge), since such a component would be killed by the projection, decreasing the norm of ρ_∞; therefore, $(\Phi_{\text{edge}} \circ \mathcal{U})[\rho_\infty] = \mathcal{U}[\rho_\infty]$. In other words, we are looking for *exactly* conserved operators of the Floquet unitary $\mathcal{U}[\rho_\infty] = \rho_\infty$ that have *no* support on the edge; obviously, this should occur only in highly contrived cases. While this argument works only for Floquet systems, where steady states can exist in a strict sense, it easily generalizes to time-dependent circuits as well: The only way for an initial state to maintain its Frobenius norm (i.e., its total purity) forever is if it *never* develops a component acting nontrivially on the edge.

Exceptions where the above argument fails are circuits with exact "blockades": unitaries where some operators are

strictly confined to a segment of the circuit not containing the edge site. The simplest example is a system that is split into decoupled subsystems at a missing bond, where $U = \mathbb{1}^{\otimes 2}$ at all times. A somewhat less trivial example is given by the Clifford toy model of MBL discussed in Ref. [103] which exhibits l-bits *exactly* localized on certain sites. Intuitively, one can understand this in the language of operator hydrodynamics [94,95,104,105]: The edge site functions as a "sink" for the operator weight which is otherwise conserved by the unitary dynamics; the only way to avoid all the weight leaving at the sink is through a strict blockade that prevents some operators from reaching the sink. Barring these fine-tuned "blockaded" circuits, the dynamics with edge decoherence Eq. (A1) always converges to the maximally mixed state. The timescale for this process, that we dub the "decoherence time" t_d, is closely related to entanglement dynamics in the unitary circuit. In localized models, as we show in Sec. III, the system takes an exponentially long time $t_d \sim \exp(L)$ to fully decohere. On the opposite end, chaotic systems take time $t_d \sim L$.

2. Normalization of the wave function

With this result in hand, we can show that the norm of a wave function $|\psi(\tilde{t})\rangle$ evolving under the nonunitary spacetime-dual circuit is statistically conserved (and exactly conserved in the thermodynamic limit $\tilde{L} \to \infty$), even though the individual gates $\tilde{U}$ are not norm preserving.

We assume the initial state $|\psi(0)\rangle$ is a product state of Bell pairs, $|B^+\rangle^{\otimes \tilde{L}/2}$, as in Fig. 3(a). Then, we aim to calculate the squared norm $\langle \psi(\tilde{t})|\psi(\tilde{t})\rangle$. The tensor network expressing this quantity is exactly the same as in Fig. 3(a), with the traced-out subsystem A encompassing the whole system. This can be interpreted from bottom to top as (i) an initial state $|B^+\rangle^{\otimes \tilde{t}/2}$ (ii) evolved with unitary gates and edge decoherence for $\tilde{\ell}$ time steps until (iii) all qubits are projected onto $\langle B^+|^{\otimes \tilde{t}/2}$. However, some care must be taken in the bookkeeping of normalizations when converting between the unitary and nonunitary arrows of time. In the nonunitary direction, the tensor network comes with a prefactor of $q^{-\tilde{\ell}/2}$: $1/q$ for every Bell-pair initial state $|B^+\rangle\langle B^+|$ (left edge). In the unitary direction, it comes with a prefactor of $q^{-\tilde{\ell}/2 - \tilde{t}}$: $1/q$ for every action of the erasure channel at the right edge and $1/q$ for every Bell pair in either the initial (bottom) or final (top) Bell states. The net result is a mismatch by $q^{-\tilde{t}}$, which must be taken into account when "flipping" the circuit.

For large systems (with $\tilde{\ell} \gg t_d$), the associated unitary-decoherence dynamics reaches the fully mixed steady state, by the very definition of the decoherence time t_d; therefore, projecting onto the final Bell-pair product state (or any other state) yields a fixed amplitude of

$$\text{Tr}[(|B^+\rangle\langle B^+|)^{\otimes \tilde{t}/2} \rho_{\text{out}}] = \langle B^+|^{\otimes \tilde{t}/2} \left(\frac{\mathbb{1}}{q}\right)^{\otimes \tilde{t}} |B^+\rangle^{\otimes \tilde{t}/2}$$

$$= q^{-\tilde{t}}.$$

This factor gets exactly canceled when converting back to the nonunitary arrow of time, so that $\langle \psi(\tilde{t})|\psi(\tilde{t})\rangle = 1$.

3. Entanglement calculation

We now consider the setup in Fig. 3(a) and show that, for the purpose of computing the entropy, it reduces to that in Fig. 3(b) in the limit of $\tilde{L} \to \infty$. We do so by splitting the tensor network that expresses the output state $|\psi\rangle$ into two pieces along the entanglement cut B:

$$\psi_{a\bar{a}} \equiv \sum_b \phi_{ab} \chi_{b\bar{a}}, \tag{A2}$$

where a and $\bar{a}$ index basis states for timelike subsystems A and $\bar{A}$, respectively, while b indexes basis states for the spacelike subsystem B at the entanglement cut (consisting of $\tilde{t}$ qubits). ϕ and χ, thus, represent the two parts of the tensor network that, when glued together at B as in Eq. (A2), yield the output wave function on $A \cup \bar{A}$.

Now, we aim to compute the entropy of the reduced density matrix on A:

$$(\rho_A)_{aa'} \equiv \sum_{\bar{a}} \psi_{a\bar{a}} \psi^*_{a'\bar{a}} = \sum_{b,b'} \phi_{ab} \phi^*_{a'b'} \left(\sum_{\bar{a}} \chi_{b\bar{a}} \chi^*_{b'\bar{a}} \right).$$

The sum in parentheses represents the reduced density matrix on B produced from running unitary dynamics with edge decoherence for a time $\tilde{L} - \tilde{\ell}$. But if $\tilde{L}$ is taken to be much bigger than the decoherence time t_d, then this density matrix is generically the identity: $\sum_{\bar{a}} \chi_{b\bar{a}} \chi^*_{b'\bar{a}} = \delta_{bb'}$ (normalizations are dealt with as above). Therefore, we have

$$\rho_A = \sum_{a,a',b} \phi_{ab} \phi^*_{a'b} |a\rangle_A \langle a'|_A. \tag{A3}$$

Finally, we can purify ρ_A to a wave function on $A \cup B$—$|\phi\rangle_{AB} \equiv \phi_{ab} |a\rangle_A \otimes |b\rangle_B$ [this is the tensor network in Fig. 3(b)]—and recover the same entropy by tracing out A instead:

$$\rho_B = \sum_{a,b,b'} \phi_{ab} \phi^*_{ab'} |b\rangle_B \langle b'|_B. \tag{A4}$$

The density matrix ρ_B is precisely the output of $\tilde{\ell}$ layers of unitary evolution and edge decoherence on $\tilde{T}$ qubits, as in Fig. 3(c) in the main text.

4. Impossibility of area-law steady states

Equipped with the results above, we can now rule out the existence of area-law entangled late-time states in all but a highly fine-tuned set of circuits. Having $|\psi(\tilde{t})\rangle$ be area-law entangled would mean that the entropy of subsystem A (of size $\tilde{\ell}$) should *not* grow with $\tilde{\ell}$ past a finite amount (independent of $\tilde{T}$ after an initial transient). But, in the edge-decoherence picture in Eq. (A4) and Fig. 3(c), this means that the mixed state $\rho_B(\tilde{\ell})$ should reach a *finite* entropy at arbitrarily large $\tilde{\ell}$. This would rule out the maximally mixed steady state $\rho_\infty = (\mathbb{1}/q)^{\otimes \tilde{t}}$ (whose entropy is $\tilde{t}$). As we see above, this is impossible in all but a set of fine-tuned blockaded circuits. This explains the absence of a "pure phase" in the model studied in Ref. [30], except for the trivial circuit consisting of $\mathbb{1}$ only (which indeed is trivially blockaded in the above sense).

APPENDIX B: DYNAMICAL PURIFICATION IN SPACETIME-DUAL CIRCUITS

In this Appendix, we study spacetime-dual circuits from the point of view of *purification dynamics* [8]: i.e., how a fully mixed initial state $\rho_{\rm in} \propto \mathbb{1}$ gradually loses entropy under the nonunitary dynamics until eventually it becomes pure, $\rho_{\rm out} = |\psi_{\rm out}\rangle\langle\psi_{\rm out}|$. The timescale for purification, t_p, exhibits a sharp phase structure: It is short $[t_p \leq O(\log L)]$ in the pure phase and long $[t_p = \exp(L)]$ in the mixed phase; the phases are separated by critical points where $t_p = {\rm poly}(L)$. These phases are closely related to the area-law and volume-law phases in pure-state dynamics, respectively [8]. In particular, the mixed phase describes the emergence of a quantum error-correcting code (QECC) capable of hiding quantum information from local measurements for very long times. Formally, this QECC is a mixed state $\rho_{\rm out}$ produced by running the nonunitary circuit on $\rho_{\rm in} \propto \mathbb{1}$ for a (polynomially) long time, $L \ll T \ll \exp(L)$ (this separation of scales is well defined only in the thermodynamic limit $L \rightarrow \infty$). $\rho_{\rm out}$ represents a stochastic superposition of all "code words," i.e., all possible pure states one may obtain as outputs by sending pure-state inputs through the circuit. Properties of this QECC have received much attention recently [42], with an appealing statistical-mechanical interpretation mapping entropies to domain-wall free energies [43]. This line of reasoning yields a conjectured universal behavior for the mutual information of the QECC $\rho_{\rm out}$ as $I_2(A:\bar{A}) = \frac{3}{2}\log|A|$ (A and $\bar{A}$ denote a contiguous bipartition of the system, shown in Fig. 10). This term also shows up as the leading correction (after the volume-law term) to the entanglement in pure-state dynamics: $S(\ell) = s\ell + \frac{3}{2}\log \ell + \cdots$. As we see, this subleading correction to the entanglement is also realized by the spacetime duals of chaotic unitary circuits in pure-state dynamics. It is thus interesting to ask whether
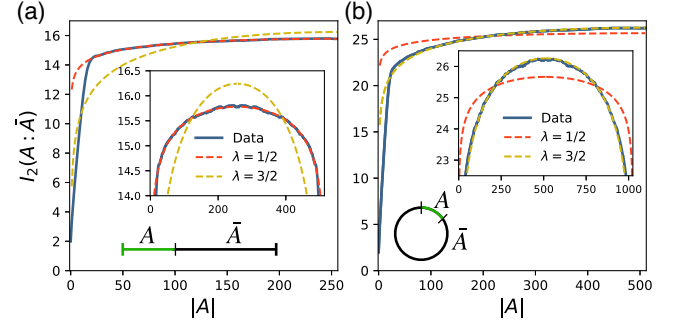

FIG. 10. Mixed purification phase in spacetime duals of Haar-random circuits. Stabilizer simulations of $\tilde{L}$ initially mixed qubits evolving under the spacetime dual of a random unitary circuit for time $\tilde{T} = 4\tilde{L}$, averaged over 6×10^5 realizations. Annealed average of the Rényi-2 "mutual information" $I_2(A:\bar{A}) = S_2(A) + S_2(\bar{A}) - S_2(A\bar{A})$, where A is a contiguous subregion that is (a) near the edge of a system with open boundary conditions or (b) in a system with periodic boundary conditions (see sketches at the bottom). In both cases, we show fits to the functions $f_\lambda(x) \equiv {\rm const} + \lambda \log_2[x(L-x)]$ with $\lambda = 1/2$ and $3/2$. The system sizes are $\tilde{L} = 512$ and 1024 in (a) and (b), respectively.

this is reflected in the mixed-state (purification) dynamics as well.

In the following, we address this question numerically. To do so, we note that our analytical discussion applies to the *annealed* average of the entropy: $S^a \equiv -\log \bar{\mathcal{P}}$, where $\mathcal{P} = {\rm Tr}(\rho^2)$ is the purity. In a spatiotemporally random circuit, ρ is a linear function of each two-qubit gate U and its adjoint $U^\dagger$; therefore, $\mathcal{P}$ is a quadratic form in U, $U^\dagger$ whose average over the unitary group is captured by a 2-design. For this reason, it is possible to compute $S^{(a)}$ by averaging over the Clifford group (which takes polynomial time through stabilizer simulations [55]) rather than the entire ${\rm U}(q^2)$ group.

For the rest of this discussion, we specialize to the case of qubits ($q = 2$) and measure entropy in bits. Given a collection of entropy samples $\{S_i\}$ from N runs of the stabilizer simulation, we have $S^{(a)} \simeq -\log_2(1/N) \sum_i 2^{-S_i}$. We note that this average may be ill conditioned if the underlying distribution of samples $P(S_i)$ has fat tails (then exponentially rare low-S samples may dominate the average); however, as we see, this is not the case for uniformly random circuits. This is also the numerical method used to obtain the data in Fig. 6 in the main text. We direct the reader to other references for details about stabilizer simulations of unitary circuits [12,55]; here, we describe only the more unusual aspect: edge decoherence. In the stabilizer formalism, the erasure channel can be implemented in two steps, first by acting with a phase-flip error and then with a bit-flip one. To do the phase-flip error, we look for any stabilizers with a Pauli X at the edge site: If there are none, nothing happens; if there is exactly one, it

is dropped from the stabilizer list; if there are several, $\{g_1, \ldots, g_k\}$, they are updated as $g'_i = g_1 g_i$ for all $i = 2, \ldots, k$, and g_1 is dropped. The bit-flip error works the same but with Z instead of X.

Numerical results are shown in Fig. 10. We find that, as in other examples of measurement-induced purification dynamics, the mutual information [127] $I_2(A:\bar{A})$ has an area-law term which grows as $\propto \log(t)$ (eventually saturating to a volume law at exponentially late times, when the output state is fully purified) and a sublinearly divergent piece. This divergent term agrees very precisely with the prediction $(k/2)\log_2 \tilde{\ell}$, with $k = 1$ if the subsystem A is near the edge of a system with open boundaries [Fig. 10(a)] and $k = 3$ if A lies in the bulk [implemented here via periodic boundary conditions; Fig. 10(b)]. Both cases are shown against fits to the symmetrized functions $f_\lambda(x) \equiv \text{const} + \lambda \log_2[x(L-x)]$, with $\lambda = 1/2$ and $3/2$.

Finally, it is interesting to examine the dynamical purification problem in the duals of "Griffiths circuits." As we argue earlier, the general understanding of the problem is that the mixed and pure phases should map onto the area-law and volume-law phases in pure-state dynamics; as the fractally entangled states arising in the duals of Griffiths circuits fit neither category, the nature of the associated purification dynamics is *a priori* unclear.

First, we note that the entropy at time $\tilde{t}$ can be bounded from above by

$$\tilde{S}(\tilde{t}) < c\tilde{L}/\tilde{t}^{1/z_p}, \tag{B1}$$

where $z_p = a + 1$ and c is a constant. This is because, after drawing a rate γ, all but $\gamma\tilde{L}$ of the system's qubits are projectively measured; thus, the state's remaining entropy is at most $\gamma\tilde{L}$. The intersection of all these bounds for time steps $1, 2, \ldots, \tilde{t}$ yields $\tilde{S} < \tilde{L} \cdot \min_{\tilde{\tau}=1,\ldots,\tilde{t}} \gamma_{\tilde{\tau}}$; as the minimum $\gamma_{\tilde{\tau}}$ typically scales as $\tilde{\tau}^{-1/(a+1)}$, we recover the bound in Eq. (B1) above.

This power-law scaling rules out a mixed phase (where purification is exponentially slow). The question is whether the power-law bound above is saturated or not. Numerical simulations of Clifford circuits with the stabilizer method answer this question in the affirmative; results are shown in Fig. 11. In particular, we find that the entropy collapses on a scaling function $\tilde{S} \simeq g(\tilde{t}/\tilde{L}^{z_p})$, with g obeying $g(x) \sim x^{-1/z_p}$ at small x [see Fig. 11(a)], which saturates the bound in Eq. (B1), before crossing over to an exponential decay e^{-cx} at large x [see Fig. 11(b)]. At $z_p = 1$ (achieved here by $a = 0$), this behavior (approximately $1/x$ to e^{-cx}) agrees with what is found generically at measurement-induced transitions, namely, collapse of the entropy onto a single-parameter dependence on the cross ratio, a signature of CFT behavior [27]. At other values of a, this family of models, thus, appears to realize a range of critical purification dynamics described by anisotropic CFTs with arbitrary $z \equiv a + 1 \in (0, \infty)$.
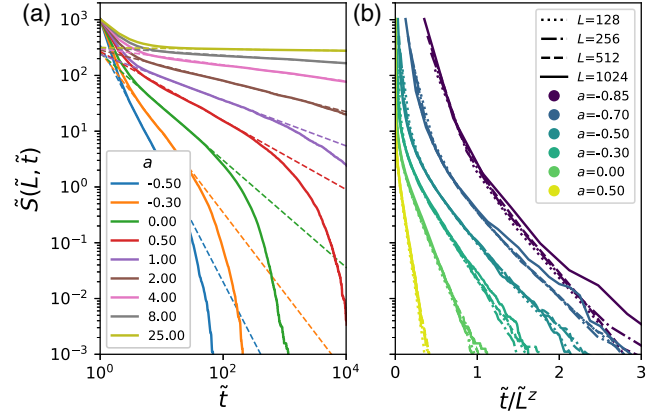

FIG. 11. Dynamical purification under the spacetime dual of the Griffiths circuit model with random Clifford gates. (a) Mixed-state entropy $\tilde{S}(\tilde{L}, \tilde{t})$ for a system of $\tilde{L} = 1024$ qubits initialized in the fully mixed state, with varying Griffiths parameter a (solid lines). At intermediate times, the entropy drops as a power law $\tilde{S}/\tilde{L} \simeq \tilde{t}^{-1/z_p}$ (dashed lines) before crossing over to an exponential form. (b) At each value of a, data for different system sizes collapse under $\tilde{t} \mapsto \tilde{t}/\tilde{L}^{z_p}$, with $z_p = a + 1$, in both the power-law and exponential decay regimes. Numerical data are obtained from stabilizer simulations and averaged over $10^3 - 10^5$ circuit realizations depending on size.

APPENDIX C: NATURE OF THE NONTHERMAL VOLUME-LAW ENTANGLED PHASE

Our results in Sec. IV and Appendix B regarding the nonthermal volume-law entangled phase in spacetime duals of chaotic unitary circuits raise an interesting question. Given that the $(3/2)\log\tilde{\ell}$ subleading correction we identify is in agreement with predictions for the analogous phase in general unitary-measurement circuits, it is natural to ask whether the two phases are the same. If so, the spacetime duals of Haar-random circuits would provide an exact microscopic realization of the "capillary wave theory" of quantum error-correcting codes presented in Ref. [43].

To address this question, we consider a distinct diagnostic introduced in Ref. [42]: the mutual information between a single qubit, located at a variable position x inside a finite subsystem A, and the (ideally infinite) complementary subsystem $\bar{A}$, $f(x) \equiv I([x]:\bar{A})$. This is a measure of how much entanglement can be destroyed by a single-site measurement inside A. Intuitively, this should be a decreasing function of x (taking $x = 0$ to be at the edge of A). For the stability of the volume-law phase in unitary-measurement circuits, $f(x)$ should decay sufficiently fast, so that its integral does not diverge [a necessary condition for measurements to destroy no more than an $O(1)$ amount of entanglement per time step, which can, in principle, be compensated by the unitary gates acting at the boundary of A]. In generic unitary-measurement circuits, this quantity is conjectured
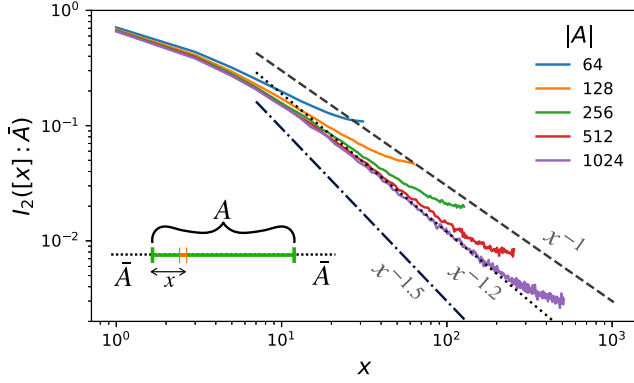
FIG. 12. Rényi-2 mutual information between a single qubit inside a contiguous region A and the (infinite) complement $\bar{A}$, as a function of the distance x between the qubit and the boundary of A. Numerical data from stabilizer simulations of the spacetime dual of a random Clifford circuit (showing only $x < |A|/2$); annealed average over $2 \times 10^4 - 5 \times 10^5$ realizations depending on size. At $|A| = 1024$, the best fit to a power-law decay is approximately $x^{-1.2}$ (dotted line), though there is a substantial finite-size drift toward larger exponents. Also shown for comparison are power laws x^{-1} (dashed line) and $x^{-1.5}$ (dot-dashed line).

to scale as $f(x) \sim x^{-3/2}$ [42], but recent work on Clifford circuits [117] finds instead $f(x) \sim x^{-1.25}$.

To compute this quantity in our setting, we consider a finite subsystem A embedded in an infinite system, initialized in a Bell-pair (pure) product state, and evolved under the dual of a random unitary circuit for a long time; in the thermodynamic limit, tracing out $\bar{A}$ yields a cancellation similar to the one we use for the pure-state entanglement calculation in Fig. 3, which elides all of the circuit except the portion contained inside a "light cone" terminating at A. One is left with a finite-size calculation on subsystem A only, with a fully mixed state and light-cone boundary conditions as in Ref. [30]. It is then possible to compute $f(x)$ from the resulting mixed state on A by exploiting the fact that $A \cup \bar{A}$ is in a pure state and using

$$f(x) = I_2([x] : \bar{A}) = S_{[x]} + S_{\bar{A}} - S_{[x] \cup \bar{A}}$$
$$= S_{[x]} + S_A - S_{A \setminus [x]}. \qquad (C1)$$

All three entropies in the expression are computable from ρ_A without reference to $\bar{A}$. Hence, our calculation implicitly takes the $\bar{A} \to \infty$ limit.

The numerical results for subsystems A of up to 1024 qubits, shown in Fig. 12, suggest that the best fit to a power law approximately $x^{-\lambda}$ is $\lambda \simeq 1.2$. This is in remarkable agreement with the results in Ref. [117], which finds an exponent $\lambda \simeq 1.25$ in an almost identical quantity, strongly suggesting that the two volume-law phases (in generic monitored circuits and in duals of chaotic circuits) are, in fact, the same.

APPENDIX D: RANDOM-WALK ENTANGLEMENT COMPUTATION FOR GRIFFITHS CIRCUITS

In this Appendix, we present results on entanglement in spacetime duals of the Griffiths circuits discussed in Sec. V based on an alternative method, which also allows us to analyze more carefully the role of corrections to scaling.

We consider the random-walk computation of the annealed average of the entanglement entropy $S^{(a)}$ for Haar-random circuits, as discussed in Sec. IV. The idea there is to take advantage of the edge decoherence picture and adapt a method developed for entanglement growth in unitary circuits, where a recursive formula [Eq. (4)] can be used to compute the purity exactly. In the Griffiths circuit model, as long as the nonidentity gates are sampled from the Haar measure, the same approach goes through, up to a small modification to the recursion: The purity $\mathcal{P}(x, t)$ is either updated as in Eq. (4) (if a gate $U \neq \mathbb{1}$ acts at bond x at time t) or left unchanged (if no gate acts). These two occurrences are weighted according to the rate γ_x of nontrivial gates acting at bond x, giving

$$\mathcal{P}(x, t) = \gamma_x \frac{q^{-v_E}}{2} [\mathcal{P}(x-1, t-1) + \mathcal{P}(x+1, t-1)]$$
$$+ (1 - \gamma_x)\mathcal{P}(x, t-1) \qquad (D1)$$

away from the decohering edge, and an analogous modification for the recursion at the edge.

We remark that evaluating this recursive formula yields the average of $\mathcal{P}$ over both the *location* (whether a gate $U \neq \mathbb{1}$ is present at bond x at time t) and *choice* [which $U \in U(q^2)$] of Haar-random gates, given the (quenched) rates γ_x. The average $\bar{\mathcal{P}}$ obtained in this way then gives an entropy $S = -\log_q \bar{\mathcal{P}}$, which can then be averaged over the choice of rates $\{\gamma_x\}$ out of the distribution $P(\gamma) = (a+1)\gamma^a$. The resulting average of S is, thus, partly annealed and partly quenched [128].

Results obtained by numerically evaluating the recursion formula on $\tilde{T} = 1024$ qubits evolving under edge decoherence are shown in Fig. 13, for qubits (the relevant case to compare to the Clifford numerics in Fig. 8) as well as systems with large local Hilbert spaces ($q = 10$), compared to the analytical prediction $\tilde{S}_\infty \sim \tilde{\ell}^\alpha$, $\alpha = (a+1)/(a+2)$. A careful look at the size dependence of $\tilde{S}$, e.g., via the logarithmic derivative $d\log(\tilde{S})/d\log(\tilde{\ell})$, reveals that the asymptotic scaling is consistent with the predicted one but that corrections to scaling are substantial for qubits, so that the best fit for the exponent in $\tilde{S} \sim \tilde{\ell}^\alpha$ is significantly off even at large sizes, $\tilde{\ell} \gtrsim 10^3$. (The data shown are for $a = 1$, where the predicted scaling is $\alpha = 2/3$ and the discrepancy with the finite-size data is worst.) This suggests that the data in Fig. 8 (from stabilizer simulations) are consistent with the analytical prediction. A more thorough investigation of subleading corrections, aiming to decouple
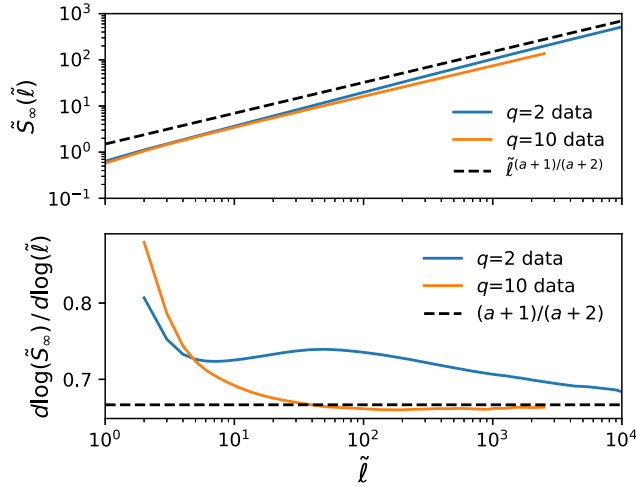
FIG. 13. Top: entropy $\tilde{S}$ vs subsystem size $\tilde{\ell}$ for the Griffiths circuit model with $a = 1$, with Haar-random gates, at depth $\tilde{T} = 1024$ (sufficient for saturation to $\tilde{S}_\infty$ at the sizes shown). The data are obtained from the recursive method, for qubits ($q = 2$) and ten-dimensional qudits ($q = 10$). Bottom: Logarithmic derivative reveals a drift of the data toward the predicted value. The corrections to scaling are large for qubits but get much smaller at large q.

the effects of (i) unitary dynamics vs edge decoherence, (ii) average over the Haar measure vs the Clifford group, and (iii) quenched vs annealed vs mixed averages, is an interesting question for future studies. In particular, it would be exciting to detect the logarithmic correction predicted for this model, though the presence of other power-law corrections due to randomness likely makes this task very hard.

[1] L. D'Alessio, Y. Kafri, A. Polkovnikov, and M. Rigol, *From Quantum Chaos and Eigenstate Thermalization to Statistical Mechanics and Thermodynamics*, Adv. Phys. **65**, 239 (2016).

[2] R. Nandkishore and D. A. Huse, *Many-Body Localization and Thermalization in Quantum Statistical Mechanics*, Annu. Rev. Condens. Matter Phys. **6**, 15 (2015).

[3] F. Harper, R. Roy, M. S. Rudner, and S. L. Sondhi, *Topology and Broken Symmetry in Floquet Systems*, Annu. Rev. Condens. Matter Phys. **11**, 345 (2020).

[4] V. Khemani, R. Moessner, and S. Sondhi, *A Brief History of Time Crystals*, arXiv:1910.10745.

[5] Y. Li, X. Chen, and M. P. A. Fisher, *Quantum Zeno Effect and the Many-Body Entanglement Transition*, Phys. Rev. B **98**, 205136 (2018).

[6] Y. Li, X. Chen, and M. P. A. Fisher, *Measurement-Driven Entanglement Transition in Hybrid Quantum Circuits*, Phys. Rev. B **100**, 134306 (2019).

[7] B. Skinner, J. Ruhman, and A. Nahum, *Measurement-Induced Phase Transitions in the Dynamics of Entanglement*, Phys. Rev. X **9**, 031009 (2019).

[8] M. J. Gullans and D. A. Huse, *Dynamical Purification Phase Transition Induced by Quantum Measurements*, Phys. Rev. X **10**, 041020 (2020).

[9] S. Choi, Y. Bao, X.-L. Qi, and E. Altman, *Quantum Error Correction in Scrambling Dynamics and Measurement-Induced Phase Transition*, Phys. Rev. Lett. **125**, 030505 (2020).

[10] A. Nahum and B. Skinner, *Entanglement and Dynamics of Diffusion-Annihilation Processes with Majorana Defects*, Phys. Rev. Research **2**, 023288 (2020).

[11] A. Lavasani, Y. Alavirad, and M. Barkeshli, *Measurement-Induced Topological Entanglement Transitions in Symmetric Random Quantum Circuits*, Nat. Phys. **17**, 342 (2021).

[12] M. Ippoliti, M. J. Gullans, S. Gopalakrishnan, D. A. Huse, and V. Khemani, *Entanglement Phase Transitions in Measurement-Only Dynamics*, Phys. Rev. X **11**, 011030 (2021).

[13] S. Sang and T. H. Hsieh, *Measurement-Protected Quantum Phases*, Phys. Rev. Research **3**, 023200 (2021).

[14] A. Lavasani, Y. Alavirad, and M. Barkeshli, *Topological Order and Criticality in* $(2 + 1)$D *Monitored Random Quantum Circuits*, Phys. Rev. Lett. **127**, 235701 (2021).

[15] J. Preskill, *Quantum Computing in the NISQ Era and Beyond*, Quantum **2**, 79 (2018).

[16] D. M. Basko, I. L. Aleiner, and B. L. Altshuler, *Metal-Insulator Transition in a Weakly Interacting Many-Electron System with Localized Single-Particle States*, Ann. Phys. (Amsterdam) **321**, 1126 (2006).

[17] D. A. Abanin, E. Altman, I. Bloch, and M. Serbyn, *Colloquium: Many-Body Localization, Thermalization, and Entanglement*, Rev. Mod. Phys. **91**, 021001 (2019).

[18] M. Žnidarič, T. Prosen, and P. Prelovšek, *Many-Body Localization in the Heisenberg XXZ Magnet in a Random Field*, Phys. Rev. B **77**, 064426 (2008).

[19] J. H. Bardarson, F. Pollmann, and J. E. Moore, *Unbounded Growth of Entanglement in Models of Many-Body Localization*, Phys. Rev. Lett. **109**, 017202 (2012).

[20] M. Serbyn, Z. Papić, and D. A. Abanin, *Universal Slow Growth of Entanglement in Interacting Strongly Disordered Systems*, Phys. Rev. Lett. **110**, 260601 (2013).

[21] K. Agarwal, S. Gopalakrishnan, M. Knap, M. Müller, and E. Demler, *Anomalous Diffusion and Griffiths Effects near the Many-Body Localization Transition*, Phys. Rev. Lett. **114**, 160401 (2015).

[22] R. Vosk, D. A. Huse, and E. Altman, *Theory of the Many-Body Localization Transition in One-Dimensional Systems*, Phys. Rev. X **5**, 031032 (2015).

[23] D. J. Luitz, N. Laflorencie, and F. Alet, *Extended Slow Dynamical Regime Close to the Many-Body Localization Transition*, Phys. Rev. B **93**, 060201(R) (2016).

[24] T. L. M. Lezama, S. Bera, and J. H. Bardarson, *Apparent Slow Dynamics in the Ergodic Phase of a Driven Many-Body Localized System without Extensive Conserved Quantities*, Phys. Rev. B **99**, 161106(R) (2019).

[25] A. Nahum, J. Ruhman, and D. A. Huse, *Dynamics of Entanglement and Transport in One-Dimensional Systems with Quenched Randomness*, Phys. Rev. B **98**, 035118 (2018).

[26] C.-M. Jian, Y.-Z. You, R. Vasseur, and A. W. W. Ludwig, *Measurement-Induced Criticality in Random Quantum Circuits*, Phys. Rev. B **101**, 104302 (2020).

[27] Y. Li, X. Chen, A. W. W. Ludwig, and M. P. A. Fisher, *Conformal Invariance and Quantum Nonlocality in Critical Hybrid Circuits*, Phys. Rev. B **104**, 104305 (2021).

[28] Y. Bao, S. Choi, and E. Altman, *Theory of the Phase Transition in Random Unitary Circuits with Measurements*, Phys. Rev. B **101**, 104301 (2020).

[29] A. Zabalo, M. J. Gullans, J. H. Wilson, S. Gopalakrishnan, D. A. Huse, and J. H. Pixley, *Critical Properties of the Measurement-Induced Transition in Random Quantum Circuits*, Phys. Rev. B **101**, 060301(R) (2020).

[30] M. Ippoliti and V. Khemani, *Postselection-Free Entanglement Dynamics via Spacetime Duality*, Phys. Rev. Lett. **126**, 060501 (2021).

[31] F. J. Wegner, *Duality in Generalized Ising Models and Phase Transitions without Local Order Parameters*, J. Math. Phys. (N.Y.) **12**, 2259 (1971).

[32] We are aware of only three special cases—critical points between noninteracting Anderson-localized phases [33–35], free fermions with fractal Fermi surfaces induced by long-range hopping [36], and Motzkin chains [37,38]— in which eigenstates can display fractional (but not fractal) entanglement scaling. Two of these are free, and all are fine-tuned points in parameter space rather than robust phases of matter. Fractal entanglement in a different sense —that of a fractal-shaped entanglement profile—has been found in the context of Floquet non-Hermitian CFTs [39].

[33] A. Kopp, X. Jia, and S. Chakravarty, *Replacing Energy by von Neumann Entropy in Quantum Phase Transitions*, Ann. Phys. (Amsterdam) **322**, 1466 (2007).

[34] X. Jia, A. R. Subramaniam, I. A. Gruzberg, and S. Chakravarty, *Entanglement Entropy and Multifractality at Localization Transitions*, Phys. Rev. B **77**, 014208 (2008).

[35] R. Nandkishore and A. C. Potter, *Marginal Anderson Localization and Many-Body Delocalization*, Phys. Rev. B **90**, 195115 (2014).

[36] G. Gori, S. Paganelli, A. Sharma, P. Sodano, and A. Trombettoni, *Explicit Hamiltonians Inducing Volume Law for Entanglement Entropy in Fermionic Lattices*, Phys. Rev. B **91**, 245138 (2015).

[37] R. Movassagh and P. W. Shor, *Supercritical Entanglement in Local Systems: Counterexample to the Area Law for Quantum Matter*, Proc. Natl. Acad. Sci. U.S.A. **113**, 13278 (2016).

[38] F. Sugino and V. Korepin, *Rényi Entropy of Highly Entangled Spin Chains*, Int. J. Mod. Phys. B **32**, 1850306 (2018).

[39] D. S. Ageev, A. A. Bagrov, and A. A. Iliasov, *Deterministic Chaos and Fractal Entropy Scaling in Floquet Conformal Field Theories*, Phys. Rev. B **103**, L100302 (2021).

[40] For example, the limit of large local Hilbert space dimension [26,28] or of all-to-all interactions [41].

[41] A. Nahum, S. Roy, B. Skinner, and J. Ruhman, *Measurement and Entanglement Phase Transitions in All-to-All Quantum Circuits, on Quantum Trees, and in Landau-Ginsburg Theory*, PRX Quantum **2**, 010352 (2021).

[42] R. Fan, S. Vijay, A. Vishwanath, and Y.-Z. You, *Self-Organized Error Correction in Random Unitary Circuits with Measurement*, Phys. Rev. B **103**, 174309 (2021).

[43] Y. Li and M. P. A. Fisher, *Statistical Mechanics of Quantum Error Correcting Codes*, Phys. Rev. B **103**, 104306 (2021).

[44] P. Ponte, Z. Papić, F. Huveneers, and D. A. Abanin, *Many-Body Localization in Periodically Driven Systems*, Phys. Rev. Lett. **114**, 140401 (2015).

[45] D. A. Abanin, W. De Roeck, and F. Huveneers, *Theory of Many-Body Localization in Periodically Driven Systems*, Ann. Phys. (Amsterdam) **372**, 1 (2016).

[46] L. Zhang, V. Khemani, and D. A. Huse, *A Floquet Model for the Many-Body Localization Transition*, Phys. Rev. B **94**, 224202 (2016).

[47] D. A. Huse, R. Nandkishore, and V. Oganesyan, *Phenomenology of Fully Many-Body-Localized Systems*, Phys. Rev. B **90**, 174202 (2014).

[48] H. Kim and D. A. Huse, *Ballistic Spreading of Entanglement in a Diffusive Nonintegrable System*, Phys. Rev. Lett. **111**, 127205 (2013).

[49] W. W. Ho and D. A. Abanin, *Entanglement Dynamics in Quantum Many-Body Systems*, Phys. Rev. B **95**, 094302 (2017).

[50] M. Mezei and D. Stanford, *On Entanglement Spreading in Chaotic Systems*, J. High Energy Phys. 05 (2017) 065.

[51] J. Dalibard, Y. Castin, and K. Mølmer, *Wave-Function Approach to Dissipative Processes in Quantum Optics*, Phys. Rev. Lett. **68**, 580 (1992).

[52] In some cases, it may by possible to overcome this barrier with the aid of classical computation, by solving a suitable "decoding" problem (for efficiently simulable evolutions, e.g., noninteracting or Clifford circuits, as well as for local probe qubits coupled to general circuits, where one can leverage locality [53,54]); however, we expect the decoding problem for the full many-body wave function to be hard in the worst case. The postselection overhead then offers a useful upper bound to the practical cost of realizing these states.

[53] M. J. Gullans and D. A. Huse, *Scalable Probes of Measurement-Induced Criticality*, Phys. Rev. Lett. **125**, 070606 (2020).

[54] C. Noel, P. Niroula, D. Zhu, A. Risinger, L. Egan, D. Biswas, M. Cetina, A. V. Gorshkov, M. J. Gullans, D. A. Huse, and C. Monroe, *Observation of Measurement-Induced Quantum Phases in a Trapped-Ion Quantum Computer*, arXiv:2106.05881.

[55] S. Aaronson and D. Gottesman, *Improved Simulation of Stabilizer Circuits*, Phys. Rev. A **70**, 052328 (2004).

[56] Y. Li, X. Chen, and M. P. A. Fisher, *Quantum Zeno Effect and the Many-Body Entanglement Transition*, Phys. Rev. B **98**, 205136 (2018).

[57] Forcing incompatible measurement outcomes results in the annihilation of the state.

[58] L. Fidkowski, J. Haah, and M. B. Hastings, *How Dynamical Quantum Memories Forget*, Quantum **5**, 382 (2021).

[59] M. Akila, D. Waltner, B. Gutkin, and T. Guhr, *Particle-Time Duality in the Kicked Ising Spin Chain*, J. Phys. A **49**, 375101 (2016).

[60] P. Kos, M. Ljubotina, and T. Prosen, *Many-Body Quantum Chaos: Analytic Connection to Random Matrix Theory*, Phys. Rev. X **8**, 021062 (2018).

[61] B. Bertini, P. Kos, and T. Prosen, *Exact Spectral Form Factor in a Minimal Model of Many-Body Quantum Chaos*, Phys. Rev. Lett. **121**, 264101 (2018).

[62] B. Bertini, P. Kos, and T. Prosen, *Entanglement Spreading in a Minimal Model of Maximal Many-Body Quantum Chaos*, Phys. Rev. X **9**, 021033 (2019).

[63] S. Gopalakrishnan and A. Lamacraft, *Unitary Circuits of Finite Depth and Infinite Width from Quantum Channels*, Phys. Rev. B **100**, 064309 (2019).

[64] B. Bertini, P. Kos, and T. Prosen, *Exact Correlation Functions for Dual-Unitary Lattice Models in $1 + 1$ Dimensions*, Phys. Rev. Lett. **123**, 210601 (2019).

[65] B. Bertini, P. Kos, and T. Prosen, *Operator Entanglement in Local Quantum Circuits I: Chaotic Dual-Unitary Circuits*, SciPost Phys. **8**, 67 (2020).

[66] L. Piroli, B. Bertini, J. I. Cirac, and T. Prosen, *Exact Dynamics in Dual-Unitary Quantum Circuits*, Phys. Rev. B **101**, 094304 (2020).

[67] P. W. Claeys and A. Lamacraft, *Maximum Velocity Quantum Circuits*, Phys. Rev. Research **2**, 033032 (2020).

[68] P. Kos, B. Bertini, and T. Prosen, *Correlations in Perturbed Dual-Unitary Circuits: Efficient Path-Integral Formula*, Phys. Rev. X **11**, 011022 (2021).

[69] M. C. Bañuls, M. B. Hastings, F. Verstraete, and J. I. Cirac, *Matrix Product States for Dynamical Simulation of Infinite Chains*, Phys. Rev. Lett. **102**, 240603 (2009).

[70] M. B. Hastings and R. Mahajan, *Connecting Entanglement in Time and Space: Improving the Folding Algorithm*, Phys. Rev. A **91**, 032306 (2015).

[71] J. Napp, R. L. La Placa, A. M. Dalzell, F. G. S. L. Brandao, and A. W. Harrow, *Efficient Classical Simulation of Random Shallow 2D Quantum Circuits*, arXiv:2001.00021.

[72] M. Foss-Feig, D. Hayes, J. M. Dreiling, C. Figgatt, J. P. Gaebler, S. A. Moses, J. M. Pino, and A. C. Potter, *Holographic Quantum Algorithms for Simulating Correlated Spin Systems*, Phys. Rev. Research **3**, 033002 (2021).

[73] S. J. Garratt and J. T. Chalker, *Many-Body Delocalization as Symmetry Breaking*, Phys. Rev. Lett. **127**, 026802 (2021).

[74] M. Sonner, A. Lerose, and D. A. Abanin, *Characterizing Many-Body Localization via Exact Disorder-Averaged Quantum Noise*, arXiv:2012.00777 [Phys. Rev. B (to be published)].

[75] A. Chan, A. De Luca, and J. T. Chalker, *Spectral Lyapunov Exponents in Chaotic and Localized Many-Body Quantum Systems*, Phys. Rev. Research **3**, 023118 (2021).

[76] A. Chan, A. De Luca, and J. T. Chalker, *Spectral Statistics in Spatially Extended Chaotic Quantum Many-Body Systems*, Phys. Rev. Lett. **121**, 060601 (2018).

[77] S. J. Garratt and J. T. Chalker, *Local Pairing of Feynman Histories in Many-Body Floquet Models*, Phys. Rev. X **11**, 021051 (2021).

[78] A. Lerose, M. Sonner, and D. A. Abanin, *Influence Matrix Approach to Many-Body Floquet Dynamics*, Phys. Rev. X **11**, 021040 (2021).

[79] A tilde is used to designate quantities in the flipped circuit.

[80] The term is inspired by quantum teleportation, where Alice and Bob share a Bell pair and Bob can perform some local operations (including measurements) to teleport a desired state to Alice's qubit. Here, too, we initialize an array of Bell pairs, feed one qudit from each pair into a unitary circuit, and then at the final time measure one part of the system to produce the desired output on the other part.

[81] A similar procedure of "swapping in" additional qubits at the edges is considered in Ref. [27].

[82] Another way of stating this is to note that open boundary conditions are equivalent to having a special bond where all gates are 1; using $\tilde{\mathbb{1}} \propto |B^+ >< B^+|$ yields the result. A subtlety with the wave function normalization is discussed in Appendix A.

[83] This argument relies on the fact that we fix $|\tilde{\psi}_{in}\rangle$ to be a product of Bell pairs. Otherwise, information could also "leak out" at the left boundary.

[84] M. A. Nielsen and I. L. Chuang, *Quantum Computation and Quantum Information: 10th Anniversary Edition* (Cambridge University Press, Cambridge, England, 2011).

[85] This is true up to some zero eigenvalues, which arise due to the fact that A and B have different sizes and do not contribute to any of the Rényi entropies.

[86] Logarithms are taken base q.

[87] In other words, those Pauli strings are killed by the edge decoherence. This also shows why the maximally mixed steady state should be unique: Other steady states would be possible only if there were operators that *never* reach the edge, e.g., if the unitary dynamics had *exactly* conserved quantities with no support at the edge. This occurs only in highly fine-tuned cases.

[88] It corresponds to the entropy of a state ρ_{BC} on a bipartite system BC, where C serves as a "reference system" for B: The two are initially in a pure, maximally entangled state, and then B evolves under unitary dynamics with edge decoherence, while C has no dynamics.

[89] V. Khemani, A. Lazarides, R. Moessner, and S. Sondhi, *Phase Structure of Driven Quantum Systems*, Phys. Rev. Lett. **116**, 250401 (2016).

[90] H. Kim, T. N. Ikeda, and D. A. Huse, *Testing Whether All Eigenstates Obey the Eigenstate Thermalization Hypothesis*, Phys. Rev. E **90**, 052105 (2014).

[91] F. Arute *et al.*, *Quantum Supremacy Using a Programmable Superconducting Processor*, Nature (London) **574**, 505 (2019).

[92] M. Ippoliti, K. Kechedzhi, R. Moessner, S. L. Sondhi, and V. Khemani, *Many-Body Physics in the NISQ Era: Quantum Programming a Discrete Time Crystal*, PRX Quantum **2**, 030346 (2021).

[93] A. Nahum, J. Ruhman, S. Vijay, and J. Haah, *Quantum Entanglement Growth under Random Unitary Dynamics*, Phys. Rev. X **7**, 031016 (2017).

[94] A. Nahum, S. Vijay, and J. Haah, *Operator Spreading in Random Unitary Circuits*, Phys. Rev. X **8**, 021014 (2018).

[95] C. W. von Keyserlingk, T. Rakovszky, F. Pollmann, and S. L. Sondhi, *Operator Hydrodynamics, OTOCs, and Entanglement Growth in Systems without Conservation Laws*, Phys. Rev. X **8**, 021013 (2018).

[96] In principle, this could differ between modes; here, we take ξ to be some characteristic typical localization length.

[97] A. Lazarides, A. Das, and R. Moessner, *Fate of Many-Body Localization under Periodic Driving*, Phys. Rev. Lett. **115**, 030402 (2015).

[98] M. Serbyn, Z. Papić, and D. A. Abanin, *Local Conservation Laws and the Structure of the Many-Body Localized States*, Phys. Rev. Lett. **111**, 127201 (2013).

[99] R. Couvreur, J. L. Jacobsen, and H. Saleur, *Entanglement in Nonunitary Quantum Critical Spin Chains*, Phys. Rev. Lett. **119**, 040601 (2017).

[100] X. Chen, Y. Li, M. P. A. Fisher, and A. Lucas, *Emergent Conformal Symmetry in Nonunitary Random Dynamics of Free Fermions*, Phys. Rev. Research **2**, 033017 (2020).

[101] G. Refael and J. E. Moore, *Entanglement Entropy of Random Quantum Critical Points in One Dimension*, Phys. Rev. Lett. **93**, 260602 (2004).

[102] N. E. Bonesteel and K. Yang, *Infinite-Randomness Fixed Points for Chains of Non-Abelian Quasiparticles*, Phys. Rev. Lett. **99**, 140405 (2007).

[103] A. Chandran and C. R. Laumann, *Semiclassical Limit for the Many-Body Localization Transition*, Phys. Rev. B **92**, 024301 (2015).

[104] V. Khemani, A. Vishwanath, and D. A. Huse, *Operator Spreading and the Emergence of Dissipative Hydrodynamics under Unitary Evolution with Conservation Laws*, Phys. Rev. X **8**, 031057 (2018).

[105] T. Rakovszky, F. Pollmann, and C. W. von Keyserlingk, *Diffusive Hydrodynamics of Out-of-Time-Ordered Correlators with Charge Conservation*, Phys. Rev. X **8**, 031058 (2018).

[106] T. Rakovszky, F. Pollmann, and C. W. von Keyserlingk, *Sub-ballistic Growth of Rényi Entropies due to Diffusion*, Phys. Rev. Lett. **122**, 250602 (2019).

[107] Throughout this section, logarithms are taken base q.

[108] The reader might worry that, in our case, we are dealing with initial states of the Bell-pair type rather than product states. Note, however, that, at any given time t, the random walker can end up only on either the even or the odd sublattice. As such, $\mathcal{P}(y, 0)$ is still the same for all y appearing in Eq. (5).

[109] Note that this is, in particular, the entanglement velocity associated with the annealed average of the second Rényi entropy—one could call it the *purity velocity* [94,110]. The rate of growth of the *quenched average*, $S_2^{(q)} \equiv \overline{S_2(t)}$, is, in general, different, although the difference is small [111]. The speeds associated to other entropies (e.g., von Neumann), on the other hand, can be significantly different [95].

[110] D. A. Rowlands and A. Lamacraft, *Noisy Coupled Qubits: Operator Spreading and the Fredrickson-Andersen Model*, Phys. Rev. B **98**, 195125 (2018).

[111] T. Zhou and A. Nahum, *Emergent Statistical Mechanics of Entanglement in Random Unitary Circuits*, Phys. Rev. B **99**, 174205 (2019).

[112] The fact that the boundary is only partially, not fully, absorbing comes about because the two states that make up the left and right halves of the domain wall are non-orthogonal: Their overlap is the factor $1/q$ picked up at the boundary.

[113] S. Redner, *A Guide to First-Passage Processes* (Cambridge University Press, Cambridge, England, 2001), 10.1017/CBO9780511606014.

[114] Since the two states $\pm$ in the partition function are not orthogonal, the domain wall does not necessarily need to return exactly to its original location. Nevertheless, random walks ending up far away are exponentially suppressed, so the overall scaling is still that of the return probability.

[115] C. Jonay, D. A. Huse, and A. Nahum, *Coarse-Grained Dynamics of Operator and State Entanglement*, arXiv:1803.00089.

[116] T. Zhou and A. Nahum, *Entanglement Membrane in Chaotic Many-Body Systems*, Phys. Rev. X **10**, 031066 (2020).

[117] Y. Li, S. Vijay, and M. P. A. Fisher, *Entanglement Domain Walls in Monitored Quantum Circuits and the Directed Polymer in a Random Environment*, arXiv:2105.13352.

[118] Y. B. Lev, G. Cohen, and D. R. Reichman, *Absence of Diffusion in an Interacting System of Spinless Fermions on a One-Dimensional Disordered Lattice*, Phys. Rev. Lett. **114**, 100601 (2015).

[119] A. C. Potter, R. Vasseur, and S. A. Parameswaran, *Universal Properties of Many-Body Delocalization Transitions*, Phys. Rev. X **5**, 031033 (2015).

[120] M. Žnidarič, Antonello Scardicchio, and Vipin Kerala Varma, *Diffusive and Subdiffusive Spin Transport in the Ergodic Phase of a Many-Body Localizable System*, Phys. Rev. Lett. **117**, 040601 (2016).

[121] T. L. M. Lezama and D. J. Luitz, *Power-Law Entanglement Growth from Typical Product States*, Phys. Rev. Research **1**, 033067 (2019).

[122] Here, we rely on the subadditivity of the von Neumann entropy: The entropy of ρ_B is upper bounded by the sum of the entropy of the cut at x_1 and the entropy of the region between x_1 and the boundary.

[123] Y. Bao, S. Choi, and E. Altman, *Symmetry Enriched Phases of Quantum Circuits*, Ann. Phys. (Amsterdam) **435**, 168618 (2021).

[124] D. A. Huse, R. Nandkishore, V. Oganesyan, A. Pal, and S. L. Sondhi, *Localization-Protected Quantum Order*, Phys. Rev. B **88**, 014206 (2013).

[125] H. C. Po, L. Fidkowski, T. Morimoto, A. C. Potter, and A. Vishwanath, *Chiral Floquet Phases of Many-Body Localized Bosons*, Phys. Rev. X **6**, 041070 (2016).

[126] T.-C. Lu and T. Grover, *Spacetime Duality between Localization Transitions and Measurement-Induced Transitions*, PRX Quantum **2**, 040319 (2021).

[127] Strictly speaking, the quantity we compute is a combination of Rényi-2 (rather than von Neumann) entropies and is, therefore, *not* valid mutual information (e.g., it can be negative).

[128] One could also average $\bar{\mathcal{P}}$ over the choice of rates, getting the overall annealed average of S, but this is statistically problematic in the model at hand, where fluctuations of purity over different choices of rates are large.